AD_____

Award Number: DAMD17-99-1-9022

TITLE: Periscopic Spine Surgery

PRINCIPAL INVESTIGATOR: Kevin R. Cleary, Ph.D.

CONTRACTING ORGANIZATION: Georgetown University
Washington, DC 20057

REPORT DATE: February 2004

TYPE OF REPORT: Annual

PREPARED FOR: U.S. Army Medical Research and Materiel Command
Fort Detrick, Maryland 21702-5012

DISTRIBUTION STATEMENT: Approved for Public Release;
Distribution Unlimited

The views, opinions and/or findings contained in this report are
those of the author(s) and should not be construed as an official
Department of the Army position, policy or decision unless so
designated by other documentation.

20040527 035

REPORT DOCUMENTATION PAGE		Form Approved OMB No. 074-0188

Public reporting burden for this collection of information is estimated to average 1 hour per response, including the time for reviewing instructions, searching existing data sources, gathering and maintaining the data needed, and completing and reviewing this collection of information. Send comments regarding this burden estimate or any other aspect of this collection of information, including suggestions for reducing this burden to Washington Headquarters Services, Directorate for Information Operations and Reports, 1215 Jefferson Davis Highway, Suite 1204, Arlington, VA 22202-4302, and to the Office of Management and Budget, Paperwork Reduction Project (0704-0188), Washington, DC 20503

1. AGENCY USE ONLY (Leave blank)	2. REPORT DATE February 2004	3. REPORT TYPE AND DATES COVERED Annual (15 Jan 2003 - 14 Jan 2004)

4. TITLE AND SUBTITLE Periscopic Spine Surgery	5. FUNDING NUMBERS DAMD17-99-1-9022

6. AUTHOR(S) Kevin R. Cleary, Ph.D.	

7. PERFORMING ORGANIZATION NAME(S) AND ADDRESS(ES) Georgetown University Washington, DC 20057 E-Mail: cleary@georgetown.edu	8. PERFORMING ORGANIZATION REPORT NUMBER

9. SPONSORING / MONITORING AGENCY NAME(S) AND ADDRESS(ES) U.S. Army Medical Research and Materiel Command Fort Detrick, Maryland 21702-5012	10. SPONSORING / MONITORING AGENCY REPORT NUMBER

11. SUPPLEMENTARY NOTES
Original contains color plates: All DTIC reproductions will be in black and white.

12a. DISTRIBUTION / AVAILABILITY STATEMENT Approved for Public Release; Distribution Unlimited	12b. DISTRIBUTION CODE

13. ABSTRACT (Maximum 200 Words)

This project is aimed at improving the state of the art of image-guided and minimally invasive procedures by developing a new generation of clinical techniques along with the computer-based hardware and software needed for their implementation.

Key research accomplishments for this year are:

- Received FDA approval to continue the clinical trail for robotically assisted spinal blocks with an additional 80 patients
- Demonstrated the feasibility of fluoroscopy serving for automatically positioning a needle driver robot at the skin entry point
- Began a new study of robotically assisted lung biopsy and demonstrated the ability to frame grap BT fluoroscopy images and display them on the robot controller
- Gathered skin motion data on four patients during CyberKnife stereotactic radiosurgery treatments under an IRB-approved protocol
- Developed a respiratory motion simulator with two 3 degree of freedom platforms to evaluate CyberKnife treatments which compensate for internal organ motion

14. SUBJECT TERMS Medical robotics, tracking, image-guided, minimally invasive, spine procedures, technology development, stereotactic radiosurgery			15. NUMBER OF PAGES 69
			16. PRICE CODE

17. SECURITY CLASSIFICATION OF REPORT Unclassified	18. SECURITY CLASSIFICATION OF THIS PAGE Unclassified	19. SECURITY CLASSIFICATION OF ABSTRACT Unclassified	20. LIMITATION OF ABSTRACT Unlimited

NSN 7540-01-280-5500

Standard Form 298 (Rev. 2-89)
Prescribed by ANSI Std. Z39-18
298-102

3 Table of Contents

4 Introduction

This project is aimed at improving the state of the art of image-guided and minimally invasive procedures by developing a new generation of clinical techniques along with the computer-based hardware and software needed for their implementation. The current focus of the project is on physician assist systems incorporating robotics, tracking, and visualization to improve the precision of instrument placement and manipulation in minimally invasive procedures. The project is led by the Imaging Sciences and Information Systems (ISIS) Center of the Department of Radiology at Georgetown University. Project collaborators include the Department of Radiation Medicine at Georgetown, the Urology Robotics Group at Johns Hopkins Medical Institutions, the NSF sponsored Engineering Research Center for Computer Integrated Surgical Systems and Technology at Johns Hopkins University, and the Engineering School at the Catholic University of America.

5 Report Body

This section describes the research accomplishments associated with each task in the statement of work. This is the fifth year report and includes research performed from 15 January 2003 to 1 February 2004. The award number is DAMD17-99-1-9022.

5.1 Task 1: Program Planning and Management

Program planning and management continues to focus on the direction of the project as well as relationships with project collaborators. Project planning and review meetings are held monthly at the ISIS Center. In the 2003 calendar year major progress was made on several projects including the development of a respiratory motion simulator for the CyberKnife radiosurgery system and new work on robotic lung biopsy. We also have begun planning for the next phase of the project, which is a related effort on the Operating Room of the Future.

We have continued our very close cooperation with both the Urology Robotics Group at Johns Hopkins Medical Institutions (lab director Dan Stoianovici, PhD) and the NSF sponsored Engineering Research Center for Computer Integrated Surgical Systems and Technology at Johns Hopkins University (center director Russell Taylor, PhD).

With the Engineering Research Center at Johns Hopkins, we have continued to financially support a PhD student (Sheng Xu). Mr. Xu has been working on the robotically assisted lung biopsy project as part of this collaborative effort. Since there is no Engineering School at Georgetown University, this provides us with a graduate student to help develop the algorithms and software for this testbed. It also allows us to leverage off the extensive medical robotics program at Johns Hopkins University.

The group continues to be very active in presenting their work at national and international conferences. Dr. Cleary is the U.S. program committee chair for the Computer Assisted Radiology and Surgery conference, which will be held in June 2004 in Chicago. Dr. Cleary organized a medical robotics workshop for the June 2003 CARS

meeting. He also organized a workshop on open source software for medical devices at the November 2003 Medical Image Computing and Computer Assisted Interventions (MICCAI) meeting. The research group also had two papers and one poster accepted at the February 2003 SPIE Medical Imaging Conference.

5.2 Task 2: Spinal Robotics
There are two subtasks under this category:
1) clinical trial of "needle driver" robot for spinal blocks
2) fluoroscopy servoing for automatic needle positioning

5.2.1 Clinical Trial of "Needle Driver" Robot for Spinal Blocks

As detailed in the last annual report, the initial clinical trial of 20 patients using the needle driver robot for spinal blocks was conducted at Georgetown University from August 2002 to December 2002. The objective of this trial is to demonstrate that a physician controlled robotic needle driver is equivalent in safety and effectiveness to the standard manual technique for needle placement in nerve and facet blocks in the perispinal region. This is a single center, randomized feasibility study that has been approved by the Georgetown Institutional Review Board, the U.S. Army Human Subjects Board, and the Food and Drug Administration (FDA).

The results have since been tabulated and were published in a paper at the Medical Imaging Computing and Computer Assisted Interventions meeting (MICCAI) in November 2003. A copy of the paper is included in the appendix [Cleary 2003][1] and the results are briefly summarized here. A picture of the robot is shown in Figure 1 and a picture of the first patient is shown in Figure 2.
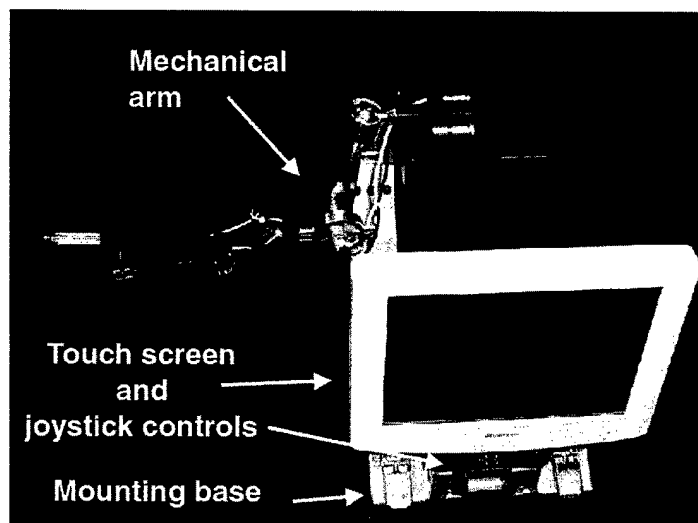

Figure 1: Robotic device showing mechanical arm and joystick control
(courtesy of Dan Stoianovici, PhD, Johns Hopkins Urology Robotics)

---

[1] All references are indicated by square brackets and listed in the reference section which is on page 17. Copies of papers are in the appendices.
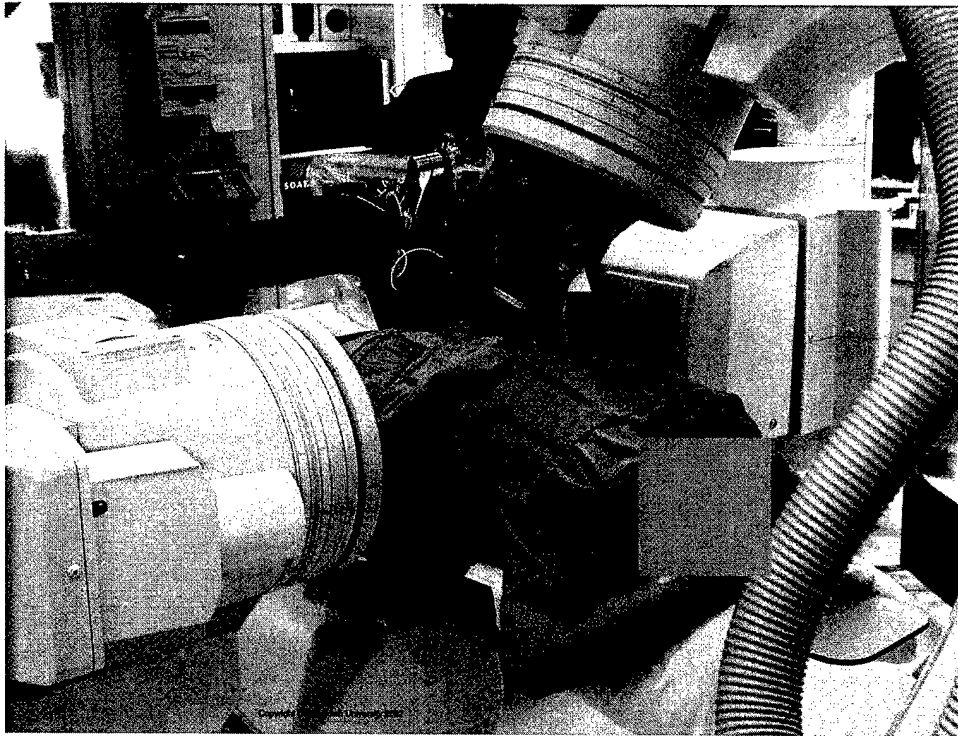
Figure 2: Clinical trial of robotic device for nerve and facet blocks at Georgetown University (interventional radiologist is Vance Watson, MD)

The clinical trial showed that is feasible to use a joystick controlled robot for nerve and facet blocks. While this was a pilot study and not enough data was gathered for statistical significance, some general trends can be observed. The mean accuracy in the robot (1.105 mm) and manual (1.238 mm) is about the same. Therefore, it appears that the robot is capable of accurate needle placement.

As expected, the pain score post-treatment was significantly less than the pain score pre-treatment in both the robot and manual arms. In the robot arm, pain scores fell from a mean of 6.3 pre-treatment to 1.8 post-treatment. In the manual arm, pain scores fell from 6.0 pre-treatment to 0.9 post-treatment. Patients had to sign an informed consent form and were generally receptive to the use of the robot.

Based on the success of this initial trial, we applied to the FDA to continue the clinical trial with an additional 80 patients. The FDA has granted approval for this and we are now working with the Georgetown and Army boards for their approval as well.

5.2.2 Fluoroscopy Servoing for Automatic Needle Positioning

The goal of this work is to develop an algorithm for automatic needle placement with the robot during minimally invasive spine procedures. This automatic needle placement is achieved by a closed-loop position control of the robot end-effector provided by a computer algorithm. The term fluoroscopy servoing is given to this process since an x-ray fluoroscope is used as the visualization tool. This work was done by Gabriela Corral of The Catholic University of America, who completed her master's thesis on this topic

in January 2004. A key contributor to this work was Luis Ibanez, PhD, of Kitware Incorporated. An extended abstract describing this work was accepted for presentation at the Computer Assisted Radiology and Surgery Meeting in Chicago in June 2004 [Corral 2004].

Figure 3 is a flow diagram of the procedure used for tracking the needle on the fluoroscopic image. First, the image is acquired using the digital frame grabber card. Using this initial image as input, a robust but relatively slow process is applied for performing an initial detection of the needle. The output of this process is a list of pixel coordinates belonging to the needle. From this set of points, a number of heuristics are applied in order to identify the tip and head of the needle. Once the initial detection is completed the robot will move and the needle will be detected. This is done until enough information is gathered to get the transformation from image to robot space to move the robot to the desire target point.
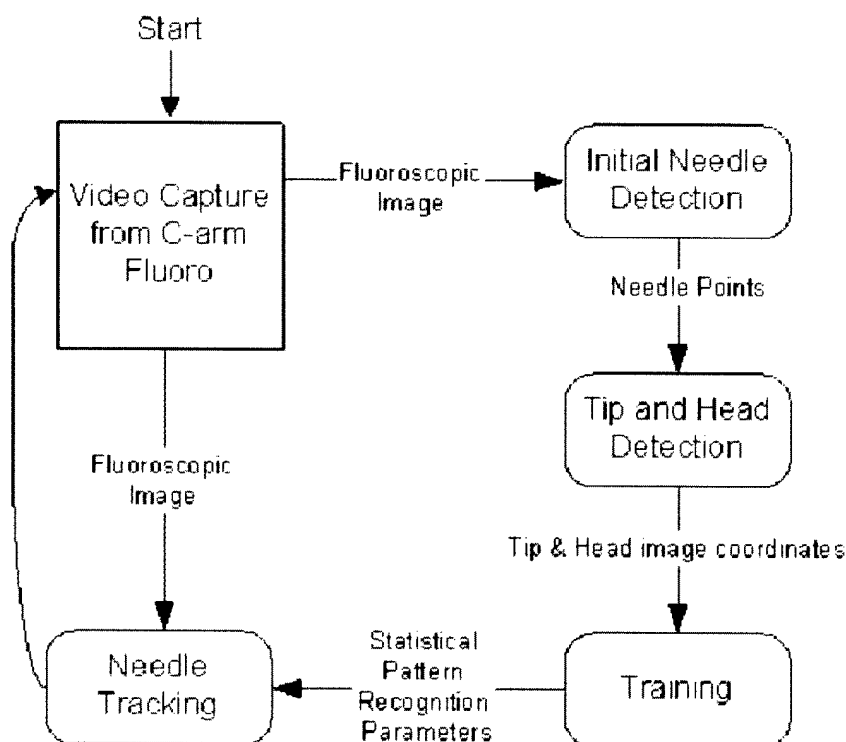

Figure 3: Flow diagram of needle tracking process

A cadaver study was performed to test the accuracy of this application. Twenty trials were performed. The difference in errors between the manual trials and the automatic trials was very small. On average the measured root mean square error for the manual trials was 1.39 +/- 1.02mm and 1.21 +/-0.66mm for the automatic trials. Both of these are clinically acceptable. We plan to continue these developments, with the eventual goal of introducing these algorithms into clinical practice.

5.3 Task 3: Robot Biopsy Testbed and Lung Biopsy

The goals of the robot biopsy testbed were:
1. to compare robotically assisted biopsy to the current practice
2. serve as a testbed for investigating software architectures for integrating robotics, tracking, and visualization.

The initial feasibility study was completed on the testbed during the last report period and paper describing the study was submitted to a special issue on Medical Robotics of the journal *IEEE Transactions on Robotics and Automation*.

While this study is complete, we have embarked on a related effort here on robotically assisted lung biopsy. This effort is also partially funded by the National Cancer Institute under grant 1 R21 CA94274-01A1. The goal of this effort is to demonstrate the feasibility of robotically assisted lung biopsy under CT fluoroscopy [Xu 2004].

In lung biopsy, the position of the target lesion may vary due to intrinsic causes such as respiratory motion or extrinsic reasons such as interactions between the tissue and a surgical tool. In developing a robotic system to assist in biopsy, we need to provide some way to track the target lesion. CT fluoroscopy combines the advantages of both CT and fluoroscopy, which offers an opportunity to track the motion of the target lesion in real-time during the intervention. Our prototype system is shown in Figure 4. The real-time CT fluoroscopy image is captured using a frame grabber (Accustream 170, Foresight Imaging, Lowell, Massachusetts, USA). The position of the target lesion is detected from the image, which serves as input for the robot controller to compensate for the motion. We have developed a motion analysis method to estimate the 3D motion of a target lesion using the CT fluoroscopy image sequences. The method aims at tracking the lesion's motion no matter whether the lesion is inside or outside the imaging plane.
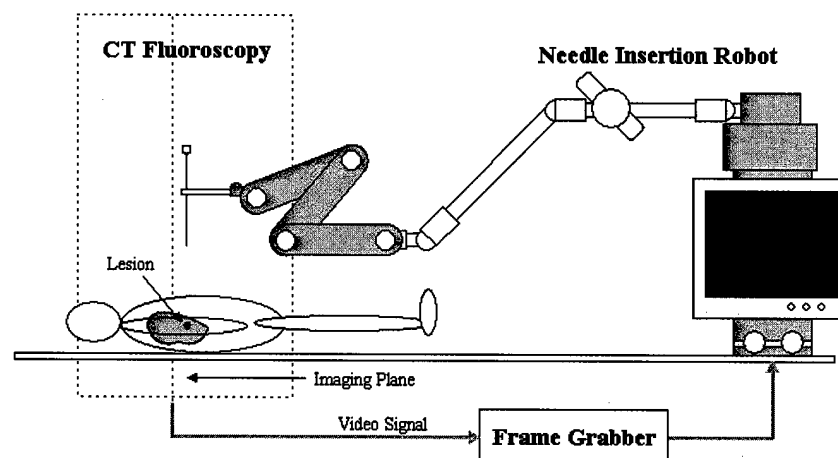

Figure 4: CT fluoroscopy guided robotically assisted lung biopsy

Three experiments were carried out using both synthetic and real CT fluoroscopy images (Siemens Somatom Volume Zoom CT). The synthetic CT fluoroscopy image was

generated from a pre-operative CT volume of the lung region with 2.0 mm slice thickness and 0.72 mm pixel size. As a result, the exact match of the CT fluoroscopy image region is known. It was observed that, for the objective function to converge, the starting point had to be within ±2mm for translation and within ±20° for each of the three rotation angles. A similar experiment was made using two different CT volumes of the same patient. With one volume as the preoperative CT volume, and the other one to generate synthetic CT fluoroscopy images, similar results were obtained.

The second experiment was performed with CT fluoroscopy images from a respiratory motion simulator. As shown in Figure 5, the target organ had one degree of freedom and was moved by a motor in the cranio-caudal direction. After a preoperative volumetric scan was obtained, the data was saved in DICOM format with 512 x 512 resolution, 1 mm slice thickness and 0.74 mm pixel size. The motor of the simulator was aligned with the CT gantry such that the motion of the phantom was perpendicular to the imaging plane (Figure 6). Since the organ phantom was rigid, its motion curve was the same as that of the motor. A sequence of CT fluoroscopy images were taken at about 6Hz and saved in the DICOM format. The resolution of the CT fluoroscopy image was 256 x 256, with 10mm slice thickness and 1.48 mm pixel size. The full details are given in the paper [Xu 2004], but the tracking results showed an average position error of under 1 mm. The third experiment was a swine study and is also described in the paper.
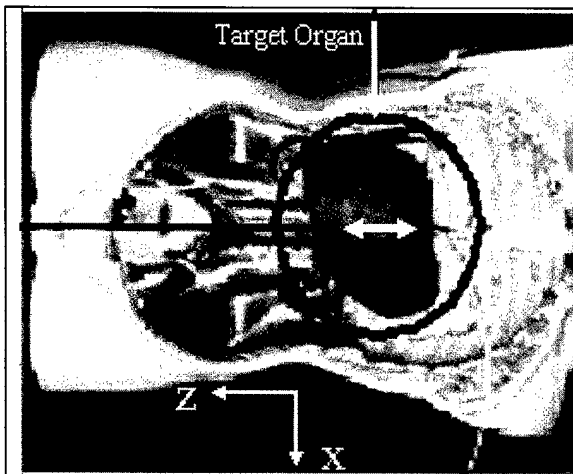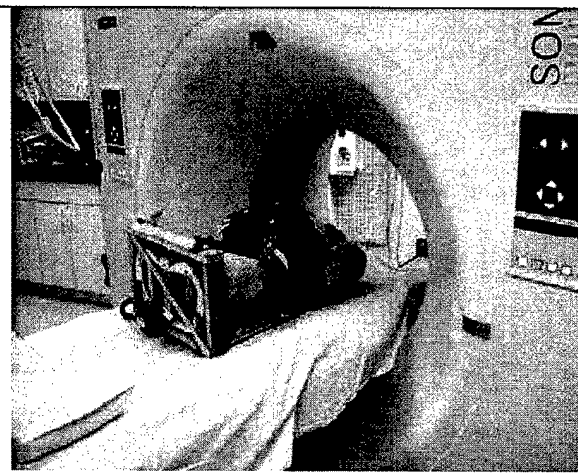

Figure 5: Respiratory motion simulator	Figure 6: Motion tracking test of respiratory motion simulator

5.4 Task 4: Liver Respiratory Motion Simulator and Internal Organ Tracking

The goal of this task is to investigate the use of electromagnetic tracking for precisely locating internal organs such as the liver during interventional procedures. This is a collaboration with Northern Digital (Waterloo, Canada) and Traxtal Technologies (Houston, Texas). Northern Digital has developed the AURORA™ electromagnetic tracking system, which enables instruments that are fitted with a sensing coil to be tracked and overlaid on an image of the anatomy. Our research group at Georgetown

served as a beta test site and was one of the first research groups worldwide to receive this equipment. The system has recently been released as a commercial product as shown in Figure 7.
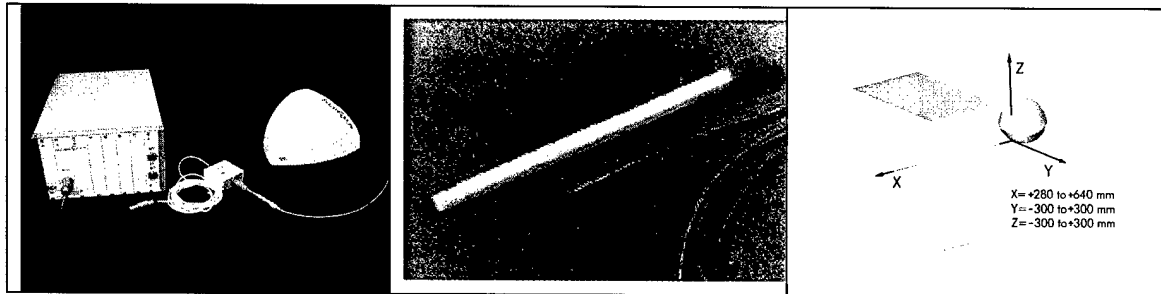

Figure 7: AURORA™ sensors, electromagnetic tracking system components, and measurement volume

The left picture shows (from left to right) the control unit, sensor interface device, and electromagnetic field generator. The middle picture shows the sensor coils along with the electrical wires protruding from the coil, compared to a match. The right picture shows the measurement volume in mm relative to the location of the field generator. (Photos courtesy of Northern Digital, Inc.)

As part of this research, we have developed an image-guided surgery system [Tang 2003]. In this system, registration is done based on pre-operative CT scans and a set of fiducials that can be localized in both image and electromagnetic space. The AURORA uses small sensor coils that can be embedded into the tip of needles or catheters to directly track their position and orientation. The system allows the physician to accurately guide a magnetically tracked needle into the abdominal area for a variety of interventional procedures that are usually done under x-ray fluoroscopy. The system has been tested on phantom torsos, respiratory motion simulators, and cadavers, all of which have been rigid-body approximations of true physiological conditions. In a liver phantom, the physician using the system has been able to target simulated liver tumors with successful placement in 14 of 16 attempts. However, the system does not perform as well with targets smaller than 1cm, deeper targets, and various other experimental conditions. This prompted us to investigate the error sources of the system.

Figure 8 shows the implementation of the system as recently used in an approved swine study in the interventional suite. The goal of this study was to hit simulated lesions in a swine liver using pre-procedure CT scans and image guidance based on electromagnetic tracking. The physician watches the image overlay shown in the lower left of the figure to manipulate the needle along a pre-planned path. Respiration is accounted for using another electromagnetically tracked needle that was placed in the liver prior to the CT scan. The current system had mixed success in accurately hitting the targets, which prompted us to investigate the sources of error in the system.

Figure 8: Swine study in the interventional suite
(interventional radiologist is Elliot Levy, MD)

The main sources of error in our rigid model include errors in electromagnetic space, image space, and human error in physical space. Figure 9 below depicts the propagation of error from electromagnetic and image space to fiducial registration and target registration.
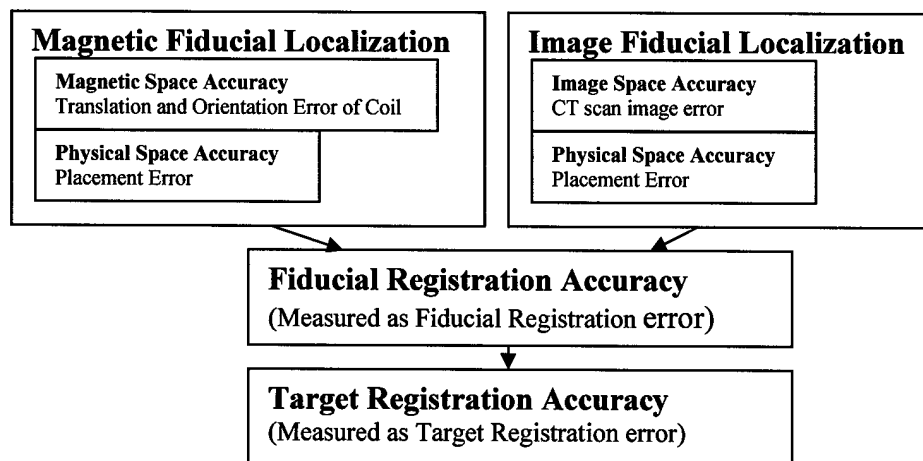
Magnetic Fiducial Localization	Image Fiducial Localization
Magnetic Space Accuracy Translation and Orientation Error of Coil	**Image Space Accuracy** CT scan image error
Physical Space Accuracy Placement Error	**Physical Space Accuracy** Placement Error

Fiducial Registration Accuracy
(Measured as Fiducial Registration error)

Target Registration Accuracy
(Measured as Target Registration error)

Figure 9: Accuracy breakdown of our registration process

We categorized the error sources into three main groups: 1) electromagnetic space, 2) CT space, and 3) physical space.

1) **Electromagnetic space.** The most obvious error source is the inherent accuracy of the electromagnetic tracking system. We use circular multi-modality fiducials (IZI Corporation, Baltimore, MD) as skin fiducials in our registration process. For the experiment described in this paper, we built a custom plexiglass registration phantom using 0.8mm tantalum beads (Tilly Medical, Sweden) as fiducials. To localize a fiducial in electromagnetic space, the center of the fiducial is touched with a magnetically tracked

probe. Error sources here include the placement error in manually localizing the center of the fiducial and error in calculating the location of the probe tip from the embedded sensor coil, which involves the combined translational and orientation error of the tracking system.

2) **CT space.** There will be some error inherent to the CT scanner and image reconstruction process but this is considered to be fairly small as we are using 1 mm slices in our experimental studies. Most of the error in localizing image fiducials will result from our manual process of choosing the center of the fiducials on the CT scan.

3) **Physical space.** In any registration procedure where manual intervention is required to select or localize the fiducials, there will always be human error. In our system, human error exists at the step where we localize the skin fiducials in electromagnetic space and image space; when the user taps out the centers of the skin fiducials on the patient and clicks on the center of the image fiducials on the CT scan. This error can not be directly measured independently from errors in the rest of our system. Errors in electromagnetic, image and physical space influenced the system's ability to accurately localize fiducials.

The results of this error analysis are detailed in the paper [Tang 2003]. There are many factors that can contribute to the overall accuracy of an image-guided surgery system based on electromagnetic tracking. A systematic analysis is necessary to isolate critical factors and determine how optimal performance can be achieved. We believe that the greatest contributor to registration error is from the manual fiducial localization process. Our simulation indicated that if we were to have a system with automatic fiducial localization, we would obtain much closer fiducial registration. This is now the focus of current research.

5.5 Task 5: Radiation Treatment
(Stereotactic Radiosurgery)

This research is being carried out in conjunction with the Radiation Medicine Department at Georgetown. A new system for precision radiation therapy (the CyberKnife) was installed at Georgetown in Spring 2002. The system includes a robotic arm which is capable of precisely positioning the radiation beam and moving it in real-time to compensate for organ motion due to respiration. Our joint research project is to investigate the use of skin motion as a predictor of internal organ motion to enhance the precision of these treatments. A protocol to collect this data during ongoing patient treatments has been approved by the Georgetown Institutional Review Board and the Army Human Subjects Research Review Board. A picture of the test setup is shown in Figure 10.
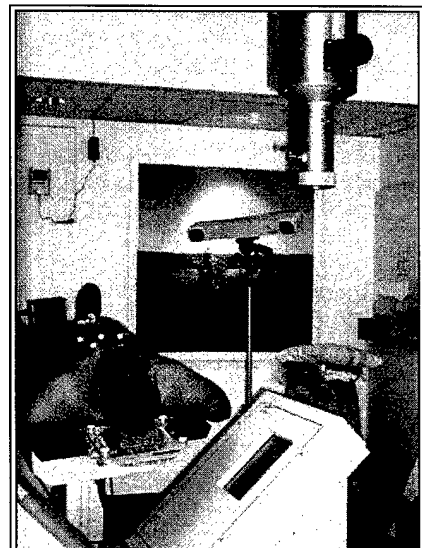

Figure 10: Example setup for tracking of skin motion data in CyberKnife suite

The results from the first four patients are given in Table 1 [Dieterich 2003a]. Two of the patients were treated in three fractions (designated by Fx in the table). Four markers were placed on the first three patients, and three markers on the fourth patient. Movement amplitudes of individual markers ranged from 3.1 mm to 14.8 mm with a median of 7.5 mm; the centroid amplitudes were between 2.1 mm and 6.0 mm. The average movement of the skin marker centroid was 4.7 mm, 3.3 mm, 2.6 mm and 6.0 mm.

Table 1: Skin marker motion for four patients

	Fx	#1 (mm)	#2 (mm)	#3 (mm)	#4 (mm)	Centroid (mm)
Patient 1	1	6.9	7.6	7.7	N/A	4.7
Patient 2	1	4.1	6.6	5.9	4.4	3.7
	2	8.0	12.2	10.9	6.2	3.4
	3	8.1	12.0	11.6	7.5	2.9
Patient 3	1	6.3	7.7	8.5	5.6	2.1
	2	6.5	5.8	7.0	4.2	2.3
	3	14.8	14.2	12.9	13.5	3.3
Patient 4	1	9.9	5.1	3.1	N/A	6.0

The centroids of the internal fiducial markers were extracted from the CyberKnife log files. The centroids moved 2.5 mm and 1.7 mm for the two patients with fiducials placed in the sacrum. The fiducial markers in the pancreas moved 3.5 mm, and 2.0 mm in the lung. There were no statistical differences in either external or internal marker movements for the first, second and third part of one treatment.

The skin motion data was then analyzed using the Fast Fourier Transformation from Matlab. Breathing patterns for a particular patient remain consistent over several treatment stages. Breathing patterns vary widely between patients; some individuals have a very consistent and predictable breathing, others show irregular breathing patterns. In general, breathing frequencies ranged from 13 Hz to 23 Hz.

Figure 11 shows the motion of the skin marker centroid of Patient 4 of our sample with the corresponding FFT analysis. The patient was diagnosed with a bronchoalveolar carcinoma of the lung and underwent multiple thoracic surgeries including upper lobectomy, right middle lobectomy, a left upper lobectomy, and right lower wedge resection. She was wearing nasal oxygen and experienced some anxiety during the treatment. While her breathing cycle is fairly regular, two distinct features could be seen from the figure. The first feature was the very high breathing rate at about 21 breaths per minute. Second, every few breaths she took a longer inhalation, which also shows two local maxima. Three examples of this can be seen in the figure at 38 s, 68 s and 78 s after the start of the recording.
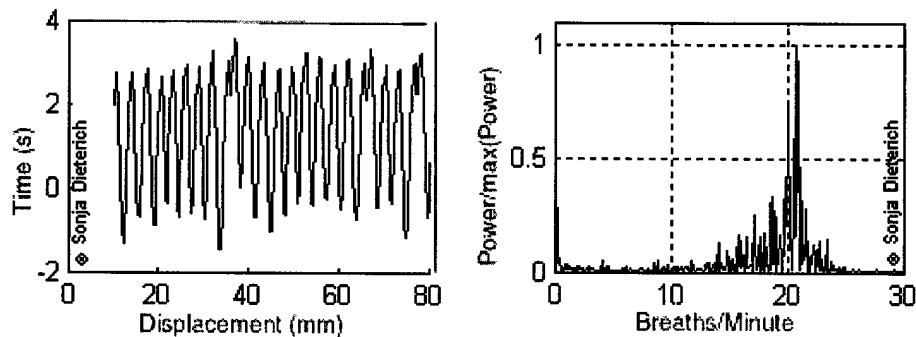
Figure 11: Motion of skin marker centroid of patient 4 (left) and FFT analysis (right)

It was found that great care needed to be taken in placing the skin markers and in arranging the environment. For example, items that reflect light such as belt buckles or shirt buttons can cause crosstalk, i.e., five instead of four skin markers were recognized. Similar problems would occur if skin markers were placed too close together. Therefore, patients were asked to wear a hospital gown for their treatment, and the markers were placed at least 10 cm apart. We also did a software cut on markers more than one meter away from the expected direction. The marker placement also was varied according to the patient's position on the treatment table (head first supine or feet first supine). For feet first supine patients, the markers were placed more inferiorly on the abdomen.

Finally, this work convinced us of the need to develop a respiratory motion simulator for the CyberKnife environment. This simulator will be used to study potential correlations between skin motion and internal organ motion and whether skin motion can be used as a predictor of internal organ motion for stereotactic radiosurgery. The simulator was designed by a local consultant, Tong Zhou, PhD, using computer aided design software as shown in Figure 12. The simulator was constructed in-house and the initial testing was done in the CyberKnife suite as shown in Figure 13. A paper was written describing the simulator which tied for first prize at the annual CyberKnife User's Group meeting [Dieterich 2003b].
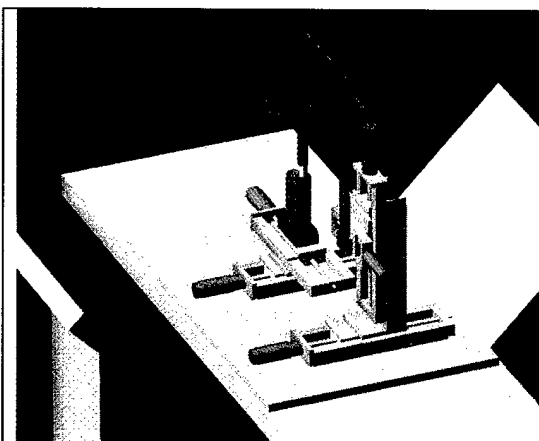

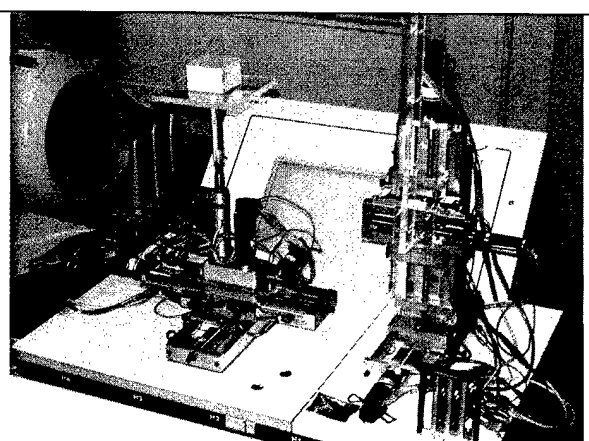| **Figure 12: Computer aided design (CAD) model of simulator on CyberKnife table** | **Figure 13: Constructed simulator during initial testing in CyberKnife suite** |

5.6 Year 6 Plans

In year 6, we plan to continue our research in three major areas:

1) robotic assistance for needle placement in the spine and lung
2) electromagnetic position sensing and guidance for abdominal interventions
3) skin motion tracking for stereotactic radiosurgery and correspondence to internal organ motion

Our overall goal remains the same: technology development to provide assistance to the physician during minimally invasive interventions. One of our project themes has been the characterization of respiratory motion and we will continue to do studies in this area. We will also continue to look for new funding opportunities and synergistic collaborations.

6 Key Research Outcomes

This section provides a bulleted list of key research accomplishments:

- Received FDA approval to continue the clinical trial for robotically assisted spinal blocks with an additional 80 patients

- Demonstrated the feasibility of fluoroscopy servoing for automatically positioning a needle driver robot at the skin entry point

- Began a new study of robotically assisted lung biopsy and demonstrated the ability to frame grab CT fluoroscopy images and display them on the robot controller

- Completed an initial set of approved animal studies demonstrating the feasibility of electromagnetic position sensing for image guidance in the interventional suite

- Gathered skin motion data on four patients during CyberKnife stereotactic radiosurgery treatments under an IRB-approved protocol

- Develop a respiratory motion simulator consisting of two 3 degree of freedom platforms to evaluate CyberKnife treatments which compensate for internal organ motion

7 Reportable Outcomes

This section provides a list of reportable outcomes.

The major product of this year is the list of papers given in Section 9, References. Copies of these documents are provided in the appendix.

In addition, several grant applications to the National Institutes of Health were submitted based on this work. Two small business Phase I grant applications were funded in 2003:
1) the first one was a STTR grant from NIH/NIBIB to Kitware Inc. to develop a software

toolkit for image-guided surgery and 2) the second one was a SBIR grant from NIH/NHLBI to Traxtal Technologies to develop electromagnetically tracked bone screws. On both of these grants, subcontracts were issued to Georgetown University for part of the research.

A graduate student from Catholic University and a graduate student from Johns Hopkins University were supported during the year to assist in software development for the robotic needle driver. The research group at Georgetown continued to take a lead in the Washington Area Computer Aided Surgery Society (www.washcas.org), which was formed in 2000 to promote research in the field.

8 Conclusions

The fifth year of work on the Periscopic Spine Surgery has continued to lay the groundwork for developing the physician assist systems of the future. These systems will incorporate robotics, tracking, and visualization to improve the precision of instrument placement and manipulation in minimally invasive procedures. Approval was received from the FDA to continue the robotic spinal blocks trial with an additional 80 patients. The feasibility of electromagnetic position sensing and image overlay was demonstrated in an animal study. A respiratory motion simulator was developed to evaluate CyberKnife treatments which compensate for internal organ motion. The focus of the next year will continue to be on technology improvements and moving this technology to clinical practice to improve patient care.

9 References

[Cleary 2003]   Cleary K, Watson V, Lindisch D, Patriciu A, Mazilu D, Stoianovici D, "Robotically assisted interventions: clinical trial for spinal blocks". *Medical Image Computing and Computer-Assisted Intervention - MICCAI 2003*, 963-964.

[Corral 2004]   Corral G, Ibanez L, Nguyen C, Stoianovici D, Navab N, Cleary K, "Robot control by fluoroscopic guidance for minimally invasive spine procedures". Accepted for presentation and publication in the proceedings at *Computer Assisted Radiology and Surgery (CARS) 2004*, Chicago, Illinois, June 23-26.

[Dieterich 2003a]   Dieterich S, Tang J, Rodgers J, and Cleary K, "Skin respiratory motion tracking for stereotactic radiosurgery using the CyberKnife". *Computer Assisted Radiology and Surgery (CARS)*, Elsevier, 2003, 130-136.

[Dieterich 2003b]   Dieterich S, Tang J, Zhou T, and Cleary K, "A programmable respiratory motion simulator for independent 3D skin and tumor motion". Paper presented at *CyberKnife User's Group Meeting*, Napa Valley, California, November 2003.

[Sacolick 2004]   Sacolick L, Patel N, Tang J, Levy E, Cleary K, "Electromagnetically tracked placement of a peripherally inserted central catheter". To be published in *Proc. SPIE Vol. 5367, Medical Imaging 2004: Visualization, Image-Guided Procedures, and Display*.

[Tang 2003]   Tang J and Cleary K, "Breakdown of tracking accuracy for electromagnetically guided abdominal interventions". *Computer Assisted Radiology and Surgery (CARS)*, Elsevier, 2003, 452-459.

[Tang 2004]   Tang J, Dieterich S, Cleary K, "Respiratory motion tracking of skin and liver in swine for CyberKnife motion compensation". To be published in *Proc. SPIE Vol. 5367, Medical Imaging 2004: Visualization, Image-Guided Procedures, and Display*.

[Xu 2004]   Xu S, Fichtinger G, Taylor RH, Cleary K, "3D motion tracking of pulmonary lesions using CT fluoroscopy image for robotically assisted lung biopsy". To be published in *Proc. SPIE Vol. 5367, Medical Imaging 2004: Visualization, Image-Guided Procedures, and Display*.

10 Appendices (Papers)

Copies of the eight papers published during this report period are reproduced in this section.

10.1 Cleary 2003: Robotically Assisted Interventions ...

Reprint begins on the next page and is 2 pages.

Robotically Assisted Interventions: Clinical Trial for Spinal Blocks

Kevin Cleary[1], Vance Watson[1], David Lindisch[1],
Alexandru Patriciu[2], Dumitru Mazilu[2], and Dan Stoianovici[2]

[1] Imaging Science and Information Systems (ISIS) Center, Department of Radiology,
Georgetown University Hospital, Washington, DC, USA
{cleary@georgetown.edu}
[2] Urobotics Laboratory, Johns Hopkins Medical Institutions, Baltimore, MD, USA

Abstract. Percutaneous interventions are performed by freehand passages of instruments, such as needles, from the skin surface to the anatomy of interest. The main problem with this approach is that the physician can be inaccurate in aligning the instrument and staying on course. A joystick-controlled robotic needle driver may allow the physician to more precisely target the anatomy. This paper describes our experience with a robotic needle driver in a 20-patient clinical trial of nerve and facet blocks. Our next stage of research in robotically assisted lung biopsy is also described.

1 Materials and Methods

The robotic needle driver consists of a three degree-of-freedom (DOF) translational stage, a 2-DOF rotational stage which can orient the needle to any angle, and a 1-DOF needle drive mechanism [1]. The robot is controlled using a joystick and touch screen. The interventionalist can thus manipulate the needle under x-ray fluoroscopy without direct exposure to the radiation beam. After cadaver studies using the robot to precisely position a needle in the lumbar spine were successfully completed [2], a randomized clinical trial of 20 patients undergoing nerve and facet blocks was approved by the FDA and the local institutional review board. The procedure is done in the standard manner except the robot is used to position, orient, and drive the needle under physician control. A/P fluoroscopy is used to position and orient the needle, and lateral fluoroscopy is used to monitor the depth of insertion.

The robot is mounted on the interventional table using a custom-designed locking mechanism. The robot is positioned initially near the skin entry point by loosening the passive gross positioning mechanism and moving the needle driver end of the robot by hand. Once this initial position has been attained, the mechanism is locked and the robot is switched to operate by physician control.

2 Results

The study was approved by the local Institutional Review Board and the Food and Drug Administration (FDA) and was conducted from August to December, 2002. The study was completed by a single fellowship trained interventional neuroradiologist at Georgetown University Hospital using a Siemens Neurostar bi-plane fluoroscopy system. The standard manual technique was used on 10 patients and the robotic device was used on 10 patients. The patients ranged in age from 30 to 70 years. The spine

levels were from S-1 to L-5. No complications were observed in the study. One of the patients in the robotics arm had to be converted to a manual procedure due to slippage of the needle driver. This conversion was done without difficulty or complications.

There were two outcome measures: 1) accuracy of needle placement and 2) pain relief. Accuracy of needle placement was determined as follows. Before the interventionalist began placing the needle, both an A/P and lateral image of the patient were obtained. The interventionalist would then annotate each image with an arrow to indicate the desired target location of the needle (the interventionalist was not blinded as to manual/robotic technique as this was not practical). After the needle was placed, an A/P and lateral image was again obtained. The two sets of images were compared to determine the distance between the intended location of the needle and the actual location of the needle. Pain relief was measured using a visual-analog scale, with 0 representing no pain and 10 representing excruciating pain.

3 Discussion

The results to date show that is feasible to use a joystick controlled robot for nerve and facet blocks. While this was a pilot study and not enough data was gathered for statistical significance, some general trends can be observed. The mean accuracy in the robot (1.105 mm) and manual (1.238 mm) is about the same. Therefore, it appears that the robot is capable of accurate needle placement.

As expected, the pain score post-treatment was significantly less than the pain score pre-treatment in both the robot and manual arms. In the robot arm, pain scores fell from a mean of 6.3 pre-treatment to 1.8 post-treatment. In the manual arm, pain scores fell from 6.0 pre-treatment to 0.9 post-treatment. Patients had to sign an informed consent form and were generally receptive to the use of the robot.

4 Future work

We are in the process of submitting our progress report to the FDA and asking for permission to enroll additional patients. In addition, the next clinical application that we are investigating is lung biopsy. The goal is to use the robotic system to assist the physician in accurate computed tomography (CT) fluoroscopy-guided needle biopsy of lung nodules.

Acknowledgements

References

1. D. Stoianovici, K. Cleary, A. Patriciu, D. Mazilu, A. Stanimir, N. Craciunoiu, V. Watson, L. Kavoussi, "AcuBot: A Robot for Radiological Interventions," accepted for publication in IEEE Transactions on Robotics and Automation, May 2003.
2. K. Cleary., D. Stoianovici, A. Patriciu, D. Mazilu, D. Lindisch and V. Watson (2002). "Robotically assisted nerve and facet blocks: a cadaveric study." Acad Radiol 9(7): 821-5.

10.2 Corral 2004: Robot Control by Fluoroscopic ...

Reprint begins on the next page and is 4 pages.

Title: Robot Control by Fluoroscopic Guidance for Minimally Invasive Spine Procedures

G. Corral(1), L. Ibanez(2), C. Nguyen(1), D. Stoianovici (3), N. Navab (4), K. Cleary(5)

(1) The Catholic University of America (USA), (2) Kitware Inc. (USA), (3) Johns Hopkins Medical Institutions, (4) Technical University of Munich, (5) Georgetown University (USA)

Purpose:

This paper describes an algorithm for automatic needle placement using a six degree of freedom (DOF) robot during minimally invasive spine procedures. This automatic needle placement is achieved by a closed-loop position control of the robot end effector provided by computer vision. The term fluoroscopy servoing is given to this process since an x-ray fluoroscope is used as the visualization tool. A software application was developed to segment the needle in the x-ray images to find its position, which is then used as feedback to control the robot and move it to a desired target point. A cadaver study was performed to test the accuracy of this application. Twenty trials were performed and the robot reached the desired target point with an average distance error of 1.21mm.

Methods:

Fluoroscopy servoing is a relatively new concept that has only been investigated by a few other researchers in the literature. Loser and Navab discuss a method of fluoroscopy servoing using a prototype that has two perpendicular rotational axes which allow 3D needle rotation around a fixed point [1]. They present an automatic image-guided control based on visual servoing, for automatic and uncalibrated needle placement under CT fluoroscopy. An initial evaluation of the robot showed an accuracy in needle placement of ±1.6mm in a small pig study. Patriciu, Stoianovici, and colleagues developed a targeting method based on a portable x-ray fluoroscope [2]. A pattern matching algorithm running on a video acquisition board is used to rapidly locate a ball marker that was placed on the needle in the x-ray image. They conducted a set of experiments in the operating room using a C-arm fluoroscope and a phantom. They used a 2mm ball as the target and placed it 80mm below the skin entry point. The maximum error over 25 experiments was less than 1.5mm.

Our goal is to move fluoroscopy servoing into clinical practice. While the papers noted above described the fluoroscopy servoing concept and did some preliminary experiments, cadaver studies were not done in the interventional environment. In addition, the work by Patriciu and Stoianovici required a ball marker on the end of the needle. Our work builds on the work of Loser and Navab and extends it to include a robust needle segmentation capability that was verified in the cadaver studies.

At Georgetown University, we recently completed a clinical trial of 20 patients using a six degree-of-freedom joystick controlled robot for needle placement for spinal nerve blocks [3, 4]. One of the first patients in this trial is shown in Figure 1 (all figures have been sent to the organizers as attachments and should be available with this abstract. In case this figure is not available, it shows the interventional radiologist using a joystick controlled needle driver robot for spinal nerve blocks). The needle placement process consists of first making a translational move to place the needle over the skin entry point, then

aligning the needle towards the nerve root, and finally driving the needle to the nerve root, all under X-ray fluoroscopy. We intend to eventually automate these steps. As a first step, in this paper we report our results in automating the translational placement of the needle at a selected skin entry point. Once the needle is at the skin entry point, we plan to apply the algorithm of Loser and Navab to align it toward the target in future work.

Our software application was written using C/C++ based libraries and toolkits. The software packages employed included:

1) Motion control library application programming interface for the robot motion control board (MEI)
2) URobotics library from Johns Hopkins. This higher level library is built on the MEI library and provides additional functionality.
3) Matrox imaging library (MIL) which provides an interface to the Matrox Meteor II frame grabber card used.
4) Fast light toolkit (FLTK) for the user interface.
5) Visualization toolkit (VTK) for image visualization and display.
6) Insight segmentation and registration toolkit (ITK) for segmentation of the needle.

Figure 2 is a flow diagram of the procedure used for tracking the needle on the fluoroscopic image. First, the image is acquired using the digital frame grabber card. Using this initial image as input, a robust but relatively slow process is applied for performing an initial detection of the needle. The output of this process is a list of pixel coordinates belonging to the needle. From this set of points, a number of heuristics are applied in order to identify the tip and head of the needle. The needle head should be interpreted as being the end of the needle opposed to the tip. The needle tip is the end that is clinically relevant here since it must be positioned at the entry point on the patient's skin. Once the initial detection is completed the robot will move and the needle will be detected. This is done until enough information is gathered to get the transformation from image to robot space to move the robot to the desire target point. The most challenging aspect of tracking the needle on the image is that at each new position the needle may be superimposed on different anatomical structures that alter the needle's intensity profile. The methods used provide a satisfactory degree of robustness against the cases of superposition commonly observed in typical clinical images. Figure 3 shows the flow diagram of the entire process used for detecting the needle in the fluoroscopic images during the calibration process.

To use the information extracted from the fluoroscopic image to guide the translational movements of the robot, we first need to determine the transform that maps the coordinate system of the robot into the image coordinate system. The direct transformation from one planar coordinate system to the other is given by a two dimensional affine transform.

To get the input for the affine transform, a calibration procedure needs to be done. This procedure establishes the relationship between the camera frame and the robot frame. The robot is moved to 3 known positions and the coordinates in both robot space and image space are recorded. Image segmentation is used to find the position of the needle in the image. These 3 point coordinates are used to compute the two dimensional transformation between the two coordinate systems.

Results:

To test the robustness of the software application two experiments were completed. The first experiment consisted of alignment of the needle under joystick control of a human operator. The second was done using the fluoroscopy servoing algorithm for automatic needle alignment. Both of these experiments were done in the interventional suite at Georgetown University using a cadaver. This was done to compare the speed and accuracy of the manual process with the automatic process. The experimental set-up is shown in Figure 4.

For the manual needle alignment a 2 mm metal BB marker was placed on the back of the cadaver and used as the target. Under continuous x-ray fluoroscopy the robot was moved by a human operator using the joystick until the needle was placed over the BB.

For the second experiment an artificial target was selected by moving the robot to an arbitrary position (to simulate a desired skin entry point). Once the robot was there the needle tip was selected as the target. At this point, the robot's position was recorded. The robot was then moved to its origin (0, 0), and the calibration process was done. When the calibration process finished, the fluoroscopy servoing algorithm was used to move the robot to the target position. The robot coordinates were then recorded at this position.

Once the 20 trials were done the x-ray images were saved in DICOM format and converted to TIFF images using a public domain software package. A typical A/P x-ray image is shown in Figure 5. Then, the measuring tool in Adobe Photoshop 5.5 was used to compute the distance from the needle tip to the center of the BB. The distance from the target to the tip of the needle was measured in the x and y directions and a root mean square distance was computed.

The difference in errors between the manual trials and the automatic trials was very small. On average the measured root mean square error for the manual trials was 1.39 +/- 1.02mm and 1.21 +/-0.66mm for the automatic trials. Both of these are clinically acceptable.

Conclusion:

This paper described the use of fluoroscopy servoing for automatic needle alignment using a medical robot. A software application was developed to frame grab the X-ray images, segment the needle, and automatically move the needle tip to a physician selected skin entry point. A cadaver study was completed in the interventional suite which showed the accuracy of automatic placement was similar to manual placement.

This is a first step in incorporating fluoroscopy servoing for automatic needle placement in clinical procedures. We intend to continue this work by adding an orientational capability and doing further validation studies before moving to a clinical trial.

References:

[1] Loser, M. and Navab, N. A new robotic system for visually controlled percutaneous interventions under CT fluoroscopy. MICCAI. 2000. Pitttsburgh, PA.

[2] Patriciu, A., Stoianovici, D., Whitcomb, L.L., Jarrett, T., Mazilu, D., Stanimir, A., Iordachita, I., Anderson, J., Taylor, R., and Kavoussi, L.R. Motion-Based Robotic Instrument Targeting under C-Arm Fluoroscopy. MICCAI. 2000. Pitttsburgh, PA.

[3] Stoianovici D, Cleary K, Patriciu A, Mazilu D, Stanimir A, Craciunoiu N, Watson V, Kavoussi L, "AcuBot: A Robot for Radiological Interventions," *IEEE Transactions on Robotics and Automation*, Oct. 2003.

[4] Cleary K, Watson V, Lindisch D, Patriciu A, Mazilu D, Stoianovici D, "Robotically Assisted Interventions: Clinical Trial for Spinal Blocks". *Medical Image Computing and Computer-Assisted Intervention - MICCAI 2003*.

10.3 Dieterich 2003a: Skin Respiratory Motion ...

Reprint begins on the next page and is 6 pages.

Skin Respiratory Motion Tracking for Stereotactic Radiosurgery using the CyberKnife

Sonja Dieterich[*], Jonathan Tang[**], James Rodgers[*], Kevin Cleary[**]

[*]Department of Radiation Oncology, Georgetown University Hospital/MedStar Health, 3800 Reservoir Road, Washington, DC, USA
[**]Imaging Science and Information Systems (ISIS) Center, Radiology Department

The purpose of this study is to report and analyze patient skin motion data collected during CyberKnife stereotactic radiosurgery. The CyberKnife is a radiation treatment system that incorporates a robotic arm to precisely position a linear accelerator. While this capability is not currently commercially available, the CyberKnife could be programmed to move the radiation beam in real-time to compensate for organ motion. This study serves as a first step towards our long-term goal of using skin motion to predict internal organ motion. This may lead to more precise radiation treatment delivery for mobile target volumes. To this date we have collected and analyzed skin motion data on four patients (two sacrum, one lung, one pancreas). The movement amplitudes of individual skin markers ranged from 3.1 mm to 14.8 mm with a median of 7.5 mm.

1. INTRODUCTION

1.1 Stereotactic Radiosurgery

Stereotactic Radiosurgery (SRS) was developed in the early 1980s with the objective of giving a high, conformal, single treatment dose to a lesion while sparing healthy tissue. The first SRS treatments were done with conventional external beam machines using multiple treatment fields and tertiary circular collimators located close to the patient. The GammaKnife used the same concept of multiple beams, but instead of a linac, the beams were generated by collimated ^{60}Co sources. Both methods, external x-ray beam and GammaKnife SRS, used forward planning to calculate target doses.

The arrival of multileaf collimators (MLCs) made it possible to change field shapes quickly and match the projection of the tumor shape. In intensity modulated radiation therapy (IMRT), this technical advancement is used to target and differentially dose sub-volumes of the lesion from multiple directions, which adds up to a conformal dose for the whole target and better avoidance of critical organs [1]. The CyberKnife (Accuray Inc., Sunnyvale, CA), while technologically very different from IMRT, employs a similar mathematical concept for dose optimization. Out of a library of about 1400 beams, the treatment planning system chooses the beams with the best target coverage and critical structure avoidance, weighing them appropriately.

The dose constraints for IMRT and CyberKnife are too complex to be handled by forward planning methods. Therefore, inverse planning algorithms were developed

starting in the late 1980s. The desired 3D dose image constraints are put in, which the algorithm mathematically inverses to calculate the output dose. Because the exact solution would include negative and imaginary intensities, in practice iterative search algorithms are used. So-called cost functions are used in most inverse planning algorithms to measure the difference between the calculated and the prescribed dose.
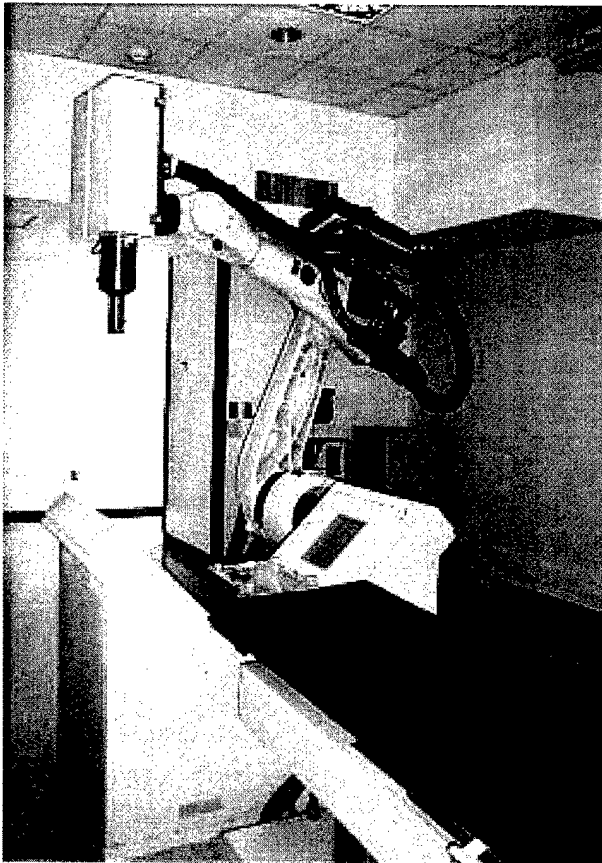
1.2 CyberKnife and Respiratory Motion

Figure 1: CyberKnife Suite at Georgetown

The CyberKnife [2,3] consists of a miniature 6 MeV linac mounted on a robot. The robot arm has a full six degrees of freedom. Two orthogonal x-ray cameras with corresponding amorphous silicon detectors allow verification of the patient's position before each treatment beam. The system automatically corrects for translations up to 10 mm. Rotational movements are displayed on the monitor and can be corrected by rotating the treatment couch, if necessary. Figure 1 shows the CyberKnife Suite in the Georgetown University Hospital Department of Radiation Medicine.

Radiation treatment of moving lesions while simultaneously sparing non-cancerous tissue has been a long-standing challenge in radiation therapy. The main focus in external beam radiotherapy has been research on breath-holding and respiratory gating techniques. While both methods have improved radiotherapy treatment, certain issues as prolonged treatment time and patient position verification have largely remain unresolved. The CyberKnife system provides the unique possibility to do real-time patient and tumor motion tracking during stereotactic radiosurgery. If the respiratory motion of a lesion could be tracked in real-time, the lesion position could be communicated via a feedback loop to the robot, which could correct for the motion. Because the high dose rate for the required treatment time makes it impractical to use fluoroscopic tracking, some researchers have used skin markers for external tracking and developed a correlation model to the internal fiducial markers. Comparing the predicted internal marker position with the position calculated by the x-ray cameras can be used for correlation model verification. Preliminary studies [4,5] using a linear correlation model have been done. Our study serves as a first step to verify those results and possibly improve respiratory motion tracking algorithms.

2. METHODS

The authors received institutional review board (IRB) approval for a study to track skin motion during regularly scheduled CyberKnife treatments. The skin motion tracking was done using a commercial infrared tracking system (Polaris, Northern Digital, Ontario, Canada). The Polaris can track the motion of non-invasive hemispherical sensors, which were temporarily attached to the patients' gown or clothing using double-sided tape. The non-invasive sensor is shown in Figure 2 and the optical tracking system is shown in Figure 3. The infrared tracking system emits infrared light that is reflected by these hemispheres. The reflections are detected by the infrared tracking system and used to determine the position of the sensors. A mock treatment session is shown in Figure 4.
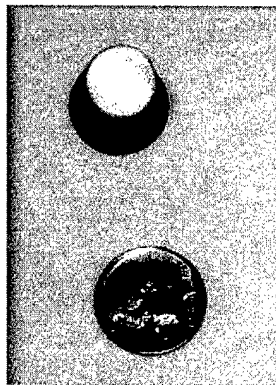
Figure 2: Non-invasive sensor compared to a dime (three or four sensors were placed on the patient)
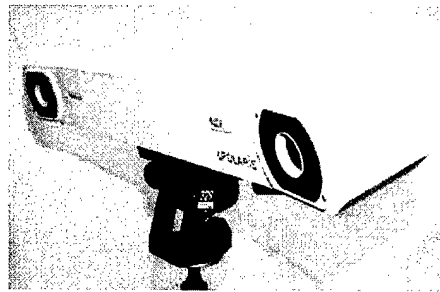
Figure 3: Infrared tracking system (placed on a tripod in the treatment room)

Figure 4: Mock treatment setup

When the patients were being prepared for treatment, the Polaris was set up in the treatment room near the foot of the table. The Polaris was controlled from a PC located outside the treatment room. The long distance between the Polaris and the PC (approximately 75 feet) required the use of the RS-422 communications standard. An adapter and special cable was required to convert the signal from its native RS-232 format. A custom software program was written to follow the position of the skin markers and save this data to disk.

Separately, the positions of the internal fiducials were recorded by the CyberKnife system and saved in log files. These internal fiducials are implanted before treatment so the CyberKnife can follow their motion using the x-ray cameras and flat

panel detectors. The internal fiducial coordinates were extracted from the log file using a Perl script and converted to a Matlab compatible file format. The skin marker coordinates were also imported into Matlab. The data was then analyzed using Matlab scripts.

3. RESULTS

Four patients have been enrolled in the study to date and the results are given in Table 1. Two of the patients were treated in three fractions (designated by Fx in the table). Four markers were placed on the first three patients, and three markers on the fourth patient. Movement amplitudes of individual markers ranged from 3.1 mm to 14.8 mm with a median of 7.5 mm; the centroid amplitudes were between 2.1 mm and 6.0 mm. The average movement of the skin marker centroid was 4.7 mm, 3.3 mm, 2.6 mm and 6.0 mm.

Table 1: Skin marker motion for four patients

	Fx	#1 (mm)	#2 (mm)	#3 (mm)	#4 (mm)	Centroid (mm)
Patient 1	1	6.9	7.6	7.7	N/A	4.7
Patient 2	1	4.1	6.6	5.9	4.4	3.7
	2	8.0	12.2	10.9	6.2	3.4
	3	8.1	12.0	11.6	7.5	2.9
Patient 3	1	6.3	7.7	8.5	5.6	2.1
	2	6.5	5.8	7.0	4.2	2.3
	3	14.8	14.2	12.9	13.5	3.3
Patient 4	1	9.9	5.1	3.1	N/A	6.0

The centroids of the internal fiducial markers were extracted from the CyberKnife log files. The centroids moved 2.5 mm and 1.7 mm for the two patients with fiducials placed in the sacrum. The fiducial markers in the pancreas moved 3.5 mm, and 2.0 mm in the lung. There were no statistical differences in either external or internal marker movements for the first, second and third part of one treatment.

The skin motion data was then analyzed using the Fast Fourier Transformation from Matlab. Breathing patterns for a particular patient remain consistent over several treatment stages. Breathing patterns vary widely between patients; some individuals have a very consistent and predictable breathing, others show irregular breathing patterns. In general, breathing frequencies ranged from 13 Hz to 23 Hz.

Figure 5 shows the motion of the skin marker centroid of Patient 4 of our sample with the corresponding FFT analysis. The patient was diagnosed with a bronchoalveolar carcinoma of the lung and underwent multiple thoracic surgeries including upper lobectomy, right middle lobectomy, a left upper lobectomy, and right lower wedge resection. She was wearing nasal oxygen and experienced some anxiety during the treatment. While her breathing cycle is fairly regular, two distinct features could be seen from Figure 5. The first feature was the very high breathing rate at about 21 breaths per minute. Second, every few breaths she took a longer inhalation, which also shows two

local maxima. Three examples of this can be seen in Figure 5a at 38 s, 68 s and 78 s after the start of the recording.
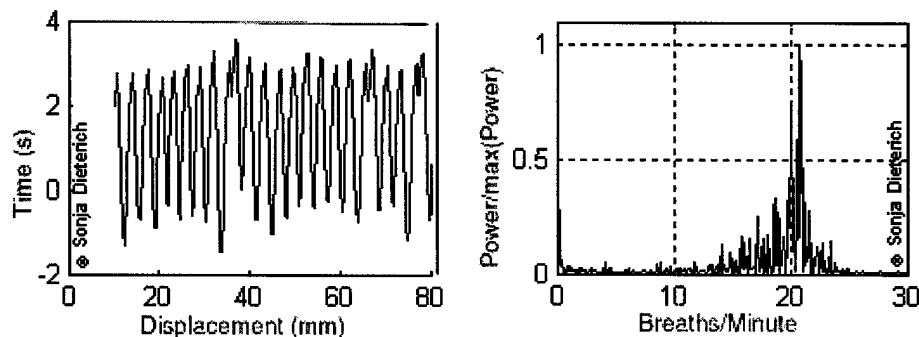

Figure 5: motion of skin marker centroid of patient 4 (left) and FFT analysis (right)

It was found that great care needed to be taken in placing the skin markers and in arranging the environment. For example, items that reflect light such as belt buckles or shirt buttons can cause crosstalk, i.e., five instead of four skin markers were recognized. Similar problems would occur if skin markers were placed too close together. Therefore, patients were asked to change into a hospital gown for their treatment, and the markers were placed at least 10 cm apart. We also chose to do a software cut on markers more than one meter away from the expected direction. The marker placement also was varied according to the patient's position on the treatment table (head first supine or feet first supine). For feet first supine patients, the markers were placed more inferiorly on the abdomen.

4. DISCUSSION

Our initial results showed that skin motion tracking with the Polaris in the CyberKnife treatment room linked to a PC outside the room is technically feasible. There was no interference of the high frequency of the CyberKnife linac with the Polaris or the signal transfer. A position for the Polaris could be found so that it is not in the way of the robotic arm and close enough to the patient to ensure stable tracking. For every patient studied, the amplitude of the skin motion was significantly larger than the tracking error of the Polaris (manufacturer's accuracy is 0.35 mm). Placing only three markers on smaller patients could minimize crosstalk between skin markers. There are still some phantom fiducials in the tracking. We assume their source is the reflection of infrared light from some not yet known reflecting surface in the treatment room. Most of the phantom markers could be eliminated by applying a software cut on all markers further than one meter from the initial marker placement.

We found that internal fiducial motion for the patients treated so far was minimal. This is in part related to the patient selection process for CyberKnife treatment. Currently, our patient population is about 50% intracranial cases, 40% spine cases and 10% non-CNS cases (paraspinal, pancreas and lung lesions attached to the mediastinum).

The CyberKnife stereotactic radiosurgery system offers new possibilities for actively compensating for respiratory motion during radiation treatment. To implement this compensation, methods need to be developed for tracking organ movement. The correlation of skin markers to internal fiducial markers is a promising tool. The complexity of breathing will require advanced methods of modeling and signal processing techniques. There is also a need to gather breathing data across a spectrum of patients, as this data is not readily available in the literature.

The data presented in this paper is intended to be a first step in these directions. We also intend to build on the work of the CyberKnife group at Stanford and their reports on skin motion and internal organ motion. The preliminary results shown here indicate that breathing patterns are complex, but that skin motion may be characterized by the centroid of the markers as the movement of the centroid was slight.

5. ACKNOWLEDGMENTS

6. REFERENCES

[1] Sternick ES, Carol MP, Grant W. Intensity-modulated Radiotherapy. In: Kahn FM, Potish RA, editors. Treatment Planning in radiation Oncology.Baltimore: Williams & Wilkins, 1998, pages.187-213.

[2] Adler JR Jr., Chang SD, Murphy MJ, Doty J, Geis P, Hancock SL; The Cyberknife: A Frameless Robotic System for Radiosurgery, Stereotact. Funct. Neurosurg. 1997, 69 (1-4 Pt 2): 124-8.

[3] Chang SD, Adler JR, Robotics and Radiosurgery – The Cyberknife, Stereotact. Funct. Neurosurg. 2001, 76 (3-4): 204-8.

[4] Murphy JM, Isaakson M, Jalden J, Adaptive filtering to predict lung tumor motion during free breathing. CARS 2002 – Lemke HU, Vannier MW; Inamura K, Farman AG, Doi K & Reiber JHC (Editors). Springer, pages 539-544.

[5] Ozhasoglu C, Murphy MJ, Issues in respiratory Motion Compensation during External Beam Radiotherapy, Int. J. Radiation Oncology Biol. Phys., Vol 52, No. 5, pp. 1389-1399 (2002).

10.4 Dieterich 2003b: A Programmable Respiratory ...

Reprint begins on the next page and is 6 pages.

A Programmable Respiratory Motion Simulator for Independent 3D Skin and Tumor Motion

S. Dieterich[a], J. Tang[b], T. Zhou[b], K. Cleary[b]

[a]Georgetown University Hospital, [b]Georgetown University Medical Center

Abstract

Introduction: With the introduction of Synchrony, the need for a programmable respiratory motion simulator (RMS) becomes apparent. The RMS can serve the multiple purposes of being used for dose delivery verification for Synchrony treatments and as a simulator to enable future technical development.

Methods: Two independent 3D motion platforms for skin (SMS) and tumor (TMS) were designed and constructed. The technical requirements for motion amplitude and speed of the respective platforms were based on patient data taken at Georgetown University Hospital (SMS) and published data (TMS). The geometry of the CyberKnife system was considered to ensure collision avoidance and avoid metal parts in the imaging area.

Results: The RMS was built completely from off-the-shelf components. Wiring, assembly and software development were done in-house and the initial tests have been completed in the CyberKnife Suite. Respiratory data taken from a lung patient treated on CyberKnife could be accurately reproduced using the simulator. Skin and liver motion data from an independent pig study could also be simulated. A film cube was treated on the RMS with and without respiratory motion. A significant difference in dose distribution for the static vs. moving (non-compensated) regular CyberKnife treatment was demonstrated.

Conclusions: The RMS can reproduce skin and tumor motion with high precision. The simulator will be used in the CyberKnife suite for phantom treatments, dose verification, and future technical developments.

1. Introduction

The CyberKnife has been used successfully for extracranial stereotactic radiosurgery [1-5] for tumors which do not show significant respiratory motion. The development of computer technology, together with the 6D motion characteristics of a robot mounted linear accelerator and advanced medical imaging, makes it technically possible to follow respiratory motion in real-time. An alternative solution, moving the leaves of a mini-multileaf collimator on external beam machines, could potentially achieve the same purpose for tumor motions perpendicular to the beams-eye view..

The challenge for both approaches lies in solving the problem of tracking the quasi-periodic motion of an internal tumor with high precision. Continuous fluoroscopy, which can be used in relatively short procedures as angiography, is not feasible for the time period required for a CyberKnife treatment. If a correlation between internal tumor motion and skin motion can be reliably established, the skin motion could be used to predict the position of the tumor. The correlation must be flexible enough to account for changes in respiratory amplitude and frequency during the treatment [6]. Typically, the respiratory rate slows down during the first few minutes of the patient lying on the treatment couch. Falling asleep, or waking up during the treatment, will change breathing patterns. Even if the system is "trained" to recognize and follow a specific patient's pattern during a fraction, inter-fractional changes may occur. If the patient experiences pain relief during the course of the treatment, intra-fraction breathing will stay unchanged, but inter-fractional breathing patterns may change. Safety requires that the system recognizes atypical patterns, such as a cough or a yawn, and stop the radiation treatment until a regular pattern is reestablished.

2. Methods and Materials

We have studied breathing patterns of patients during CyberKnife treatment using the Polaris infrared tracking system (Northern Digital, Ontario, Canada) under an IRB approved protocol. Because patients are selected with tumors which do not move much or at all with respiratory motion, there was no correlation to internal fiducial markers to be established. However, we were able to study respiratory motion amplitudes, skin marker deformation, intra- and inter-fractional changes of breathing patterns for a wide variety of patients [7]. The next step is to develop algorithms to predict the direction of skin marker motion 250 ms ahead, which corresponds to the CyberKnife system response time for a Synchrony treatment. To test the algorithms, we plan to use of respiratory motion data taken during animal studies. Therefore, we decided to build a respiratory motion simulator (RMS).

A respiratory motion simulator for the CyberKnife should have two independent stages capable of 3D movement for internal and skin movements. Both stages, the tumor motion simulator (TMS) and the skin motion simulator (SMS), should be programmable with

real patient motion data taken during CyberKnife treatments. Because a RMS could be used as a dose verification phantom for Synchrony treatments, the TMS should be able to carry the weight of a film cube enclosed in a dose buildup material. No metal should be in the imaging region to allow for fiducial tracking. The overall size is limited by the treatment table, safety box (robot/RMS collision avoidance) and no-metal zone. The relative position accuracy should be better than 0.2 mm. The maximum breathing amplitudes are 3 cm in all directions and the maximum breathing frequency is 30 breaths per minute. The external load for the TMS is 5 kg; the SMS does not carry load. The weight of each platform is approximately 12 kg.
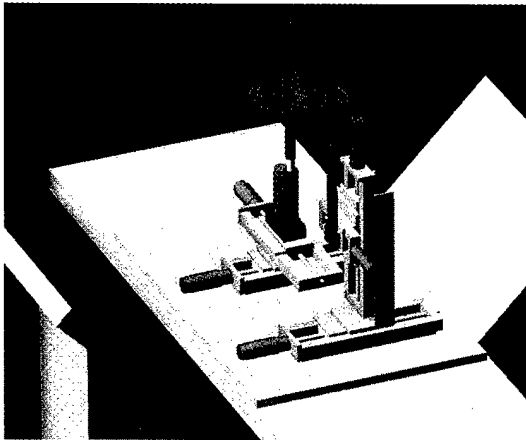
Figure 1: CAD model of RMS
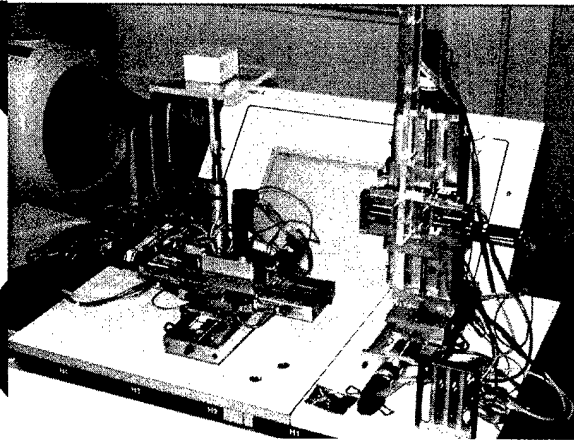
Figure 2: RMS in Cyberknife Suite

The SMS uses three linear slides (Velmex) to provide motion on three axes. The TMS uses two linear slides for the first two axes, and a linear actuator for the third axis. Each axis is driven by a motor, optical encoder, and gearhead assembly (Maxon). The combination of motor, optical encoder and gearhead is accurate to 1/9600 revolutions of the motor, which corresponds to a resolution of 0.001mm on the sliders. The motion simulator is controlled by a six axes standalone Motion Control Card (Galil) that can be commanded from outside the treatment room via Ethernet.
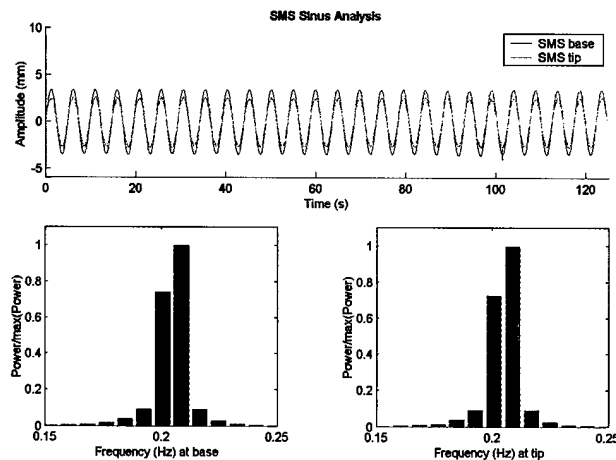
Figure 3: Skin marker on base and tip of the SMS stage were moved in a sinusoidal motion. A frequency analysis was done to check for vibrations.

3. Results

The RMS was tested in the CyberKnife Suite. First, we separately tested both stages with a 3D sinusoidal motion. The motion programmed motion frequency was 0.2 Hz. Two fiducial markers were used on each stage: one on the bases of the motion, and the second one on the phantom platform/tip of the beam. The data was analyzed for vibration, position accuracy and timing. Figure 3 shows the results for the SMS stage.

These tests were followed by a 16 minute breathing motion reproduction of skin respiratory motion data from a CyberKnife patient treatment for both stages. The data used was the centroid of four fiducials placed on this patient's abdomen.
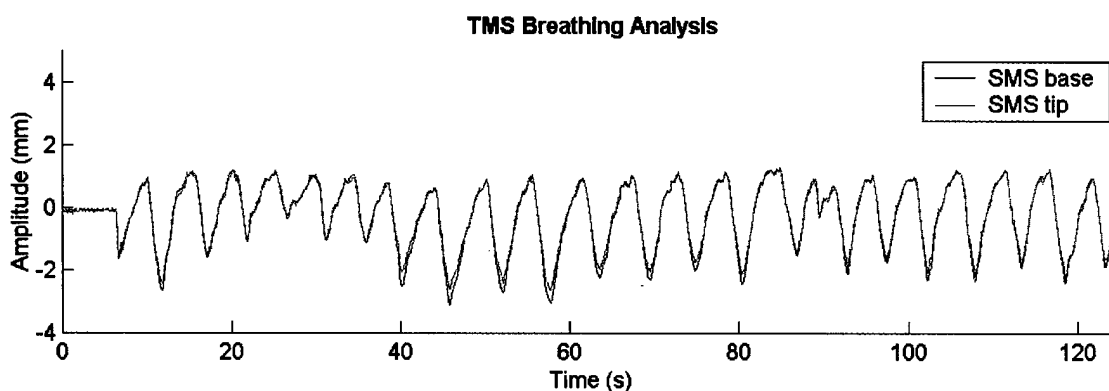
Figure 4

The RMS was then run with skin and liver motion data from a pig study. Both stages could be run, and no collision problems between the two stages occurred. Several x-ray images of a film cube placed on the TMS platform were taken with the CyberKnife image system. No metal showed in the vicinity of the fiducials within the film block. Parts of the motor of the lowest TMS linear slider showed at the periphery of the Camera A image, which will not interfere with fiducial tracking within the range of TMS motion.
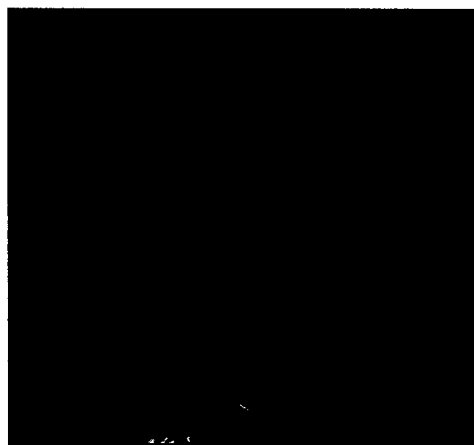
To demonstrate the distortions of dose distributions in a tumor for uncorrected breathing motion, we did two phantom treatments. The film cube was loaded with two sheets of GaFchromic film placed perpendicularly to each other. A CT of the film cube on the TMS platform was taken and transferred to the CyberKnife. A spherical tumor was contoured and planned with a dose of 3000 cGy to the 80% isodose line. Three fractions of this treatment were delivered. For the first fraction, the film cube was aligned and treated with no motion at all. Imaging was disabled; therefore no motion compensation was done. For the second fraction we moved the TMS in a sinus motion with 5 mm amplitude in the anterior-posterior and left-right direction and 10 mm in the inferior-superior direction. The phantom was imaged before every treatment beam and CyberKnife then corrected for translational shifts.
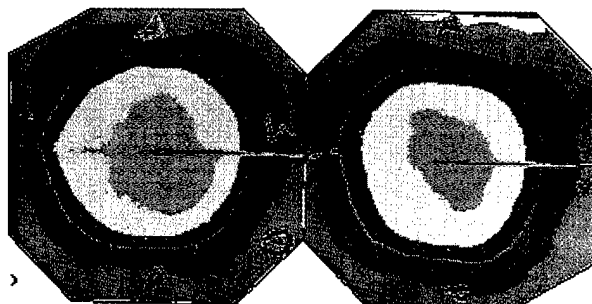
Figure 5: Digitized film of the sagittal plane without (left) and with (right) sinusoidal TMS
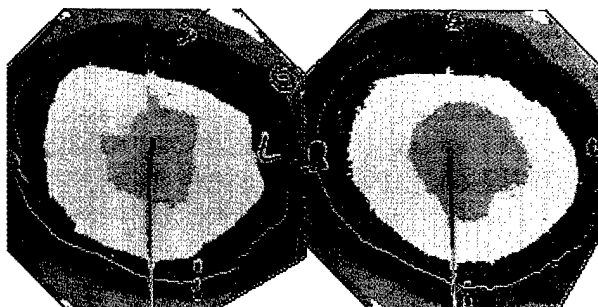
Figure 6: Digitized film of the coronal plane without (left) and with (right) sinuisoidal TMS motion.

4. Conclusion

The RMS fits the physical space requirements and we have completed initial testing in the CyberKnife Suite. Both stages can be independently programmed to reproduce patient and pig data. No metal parts interfered with fiducial tracking of a phantom on the TMS platform. The phantom could be run from the CyberKnife treatment console during beam delivery. The basic hardware design fulfilled our expectation. Small changes, e.g. a less vibrating SMS beam and further improvement of the software, will be done. The RMS can reproduce skin and tumor motion with high precision. The simulator will be used in the CyberKnife suite for phantom treatments, dose verification and future technical developments.

5. Acknowledgments

6. References/ Literature

[1] Gerszten, P.C., Ozhasoglu, C., Burton, S.A., Vogel, W.J., Atkins, B.A., Kalnicki, S., Welch, W.C.: CyberKnife frameless single-fraction stereotactic radiosurgery for benign tumors of the spine. *Neurosurgical Focus* (5):Article 16, 2003.

[2] Gerszten, P.C., Ozhasoglu, C., Burton, S.A., Welch, W.C., Vogel, W.J., Atkins, B.A., Kalnicki, S.: CyberKnife frameless single-fraction stereotactic radiosurgery for tumors of the sacrum. *Neurosurgical Focus* 15(2): article 7, 2003.

[3] Gibbs, I.C., Chang S.D.: Radiosurgery and radiotherapy for sacral tumors. *Neurosurgical Focus* 15(2):article 8, 2003.

[4] Whyte RI, Crownover R, Murphy MJ, Martin DP, Rice TW, DeCamp MM Jr, Rodebaugh R, Weinhous MS, Le QT. : Stereotactic radiosurgery for lung tumors: preliminary report of a phase I trial. *Ann Thorac Surgery* 75(4):1097-101, 2003.

[5] Murphy MJ, Martin D, Whyte R, Hai J, Ozhasoglu C, Le QT: The effectiveness of breath-holding to stabilize lung and pancreas tumors during radiosurgery. *International Journal of Radiation Oncology Biology Physics* 53(2):475-82, 2002.

[6] Ozhasoglu C, Murphy MJ, Issues in respiratory Motion Compensation during External Beam Radiotherapy, Int. J. Radiation Oncology Biol. Phys., Vol 52, No. 5, pp. 1389-1399 (2002).

[7] Dieterich S, Tang J, Rodgers J, Cleary K: Skin respiratory motion tracking for stereotactic radiosurgery using the CyberKnife. CARS 2003 – Lemke HU, Vannier MW; Inamura K, Farman AG, Doi K & Reiber JHC (Editors). Springer.

10.5 Sacolick 2004: Electromagnetically tracked ...

Reprint begins on the next page and is 5 pages.

Electromagnetically tracked placement of a peripherally inserted central catheter

Laura Sacolick[a], Neilesh Patel[a], John Tang[b], Elliot Levy[c], Kevin Cleary[b*]

[a]Johns Hopkins University, Dept. of Biomedical Engineering, Baltimore, MD, USA
[b]Imaging Science and Information Systems (ISIS) Center, Dept. of Radiology,
Georgetown University, Washington, DC, USA
[c]Georgetown University Hospital/MedStar Health, Washington, DC, USA

ABSTRACT

This paper describes a computer program to utilize electromagnetic tracking guidance during insertion of peripherally inserted central catheters. Placement of a Peripherally Inserted Central Catheter (PICC) line is a relatively simple, routine procedure in which a catheter is inserted into the veins of the lower arm and threaded up the arm to the vena cava to sit just above the heart. However, the procedure requires x-ray verification of the catheter position and is usually done under continuous fluoroscopic guidance. The computer program is designed to replace fluoroscopic guidance in this procedure and make PICC line placement a bedside procedure. This would greatly reduce the time and resources dedicated to this procedure. The physician first goes through a quick registration procedure to register the patient space with the computer screen coordinates. Once registration is completed, the program provides a continuous, real-time display of the position of the catheter tip overlaid on an x-ray image of the patient on an adjacent computer screen. Both the position and orientation of the catheter tip is shown. The display is very similar to that shown when using fluoroscopy.

Keywords: electromagnetic tracking, PICC, catheter insertion

1. INTRODUCTION

The peripherally inserted central catheter line is often used in patients requiring long term or home intravenous access for a wide variety of medical conditions. It is inserted in the lower arm, feeds up the subclavian vein, then the brachiocephalic vein, and finally it enters the superior vena cava. It does not become as easily infected or dislodged as a shorter intravenous line and is safer to insert and take care of than a central venous catheter (CVC) line. Although the PICC line is a long-term use catheter, it must be changed if it becomes infected or remains in the patient too long. The procedure is carried out fairly often for a variety of treatments. For these reasons, PICC line insertion is a procedure done many times a day in every hospital, and requires a fair amount of hospital resources and time.

Electromagnetic guidance is a modality that may be useful for guiding minimally invasive surgical procedures. It can provide accurate tracking without the line-of sight requirements of optical trackers. This characteristic makes it possible to use electromagnetic tracking systems for tracking surgical implements inside the body without an open incision. For instance, electromagnetic guidance of catheters is currently used in minimally invasive cardiac surgery [1]. Our research group is investigating using electromagnetic tracking for applications as diverse as needle placement, RF ablation, and organ motion tracking [1][2][4][5].

*Contact information: cleary@georgetown.edu, phone (202) 687-8253, fax (202) 784-3479

For our system, we have chosen to use the AURORA Electromagnetic Tracker (Northern Digital, Inc, Waterloo, Canada, Figure 1). The AURORA consists of a field generator (right hand side of Figure 1), a control unit (left hand side of Figure 1), and small coil sensors that can be embedded in catheters, needles, and other instruments. The coils return the sensor position and orientation with five degrees of freedom (x, y, z translations and two orientations). It has been demonstrated to give reasonably good accuracy [6], is small, reasonably priced, and easily portable. Using this method of guidance could greatly cut down on the number of PICC line cases that would need access to fluoroscopy equipment.

Figure 1: AURORA control unit and field generator
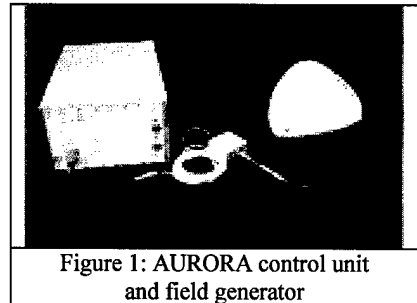
2. METHODS

2.1 PICC Placement

The procedure for inserting a PICC line is very simple. The physician needs to see that the catheter goes up the subclavian vein, then the brachiocephalic vein, and ends up in the superior vena cava. There are basically two possible problems with the procedure which would have to be easily recognizable by our system. The physician must be able to recognize if the catheter takes a path into a wrong vein. For instance, the catheter may go up into the jugular vein instead of the vena cava, or miss the vena cava and pass across to the other side of the body. The physician must also be able to see if the catheter becomes stuck in a vein or doubles back on itself.

Fluoroscopic guidance gives a very good view of exactly where the catheter is in the patient's anatomy at any time. However, it exposes the patient to some amount of radiation. Our goal was to use electromagnetic tracking to give the physician a view similar to what he would see with digital fluoroscopy, but without the radiation. We consulted with an interventional radiologist experienced in the procedure, and were given the following requirements for our system. Our program must run in real time and update often enough to give the physician continuous information about the location of the catheter. The display must show the path and location of the catheter clearly enough to detect its taking a wrong path or getting stuck in a vein. In addition to this, the system is portable and able to be run off a laptop computer and can be moved into any patient's room.

2.2 Software Design

Since this project was begun by students as part of a class at Johns Hopkins University, our program relies on the open source Computer Integrated Surgery C++ library developed by the Engineering Research Center at Johns Hopkins. This software is used for the AURORA drivers as well as the code for mathematical operations such as calculation of frame transformations. The software is also dependent on the Fast Light Toolkit 1.10 (FLTK) for the graphical display and user interface control.

The first step in the procedure for using our software is to perform a pivot calibration of the catheter. In the electromagnetically tracked catheters that were used for this project, the sensor coil was not necessarily in the tip of the catheter, but may be offset by as much as 1-2 mm. The physician is asked to take 6 readings with the catheter tip touching a single point at different orientations. From this, the average distance is calculated from the coil to the physical tip of the catheter. Data from the pivot calibration can be saved and reloaded if the physician would like to reuse the catheter.

In the interest of keeping the format of the display similar to the fluoroscopy display that the physician is accustomed to, the catheter location is overlaid on a chest x-ray image of the patient. Patients that require a PICC line often have other medical problems and in the past, may have needed a chest x-ray. The program allows the physician to load either a patient-specific x-ray or a generic x-ray from a collection of images.

The next step in our software is to perform a simple registration procedure to get the coordinate frame transformation from the three-dimensional AURORA coordinates to the two-dimensional image space on the computer screen. From this point through the rest of the procedure, it is necessary to keep the patient from moving on the table. With the mouse pointer, the user is asked to click on the fiducial points on the screen that he intends to use. Basically any points on the body that can be readily identified on both the chest x-ray and the outside of the patient's body can be used as fiducial

points. We recommend using the sternal notch, xiphoid process, and the acromioclavicular junction on each side (shoulders) as four easily found fiducial points (Figure 2). At least three points are necessary for registration, but the physician may use as many as he chooses.

The physician then touches the tip of the catheter to the corresponding fiducial points on the patient's body. When this is complete, the result is the frame transformation from patient space to image coordinates. At this point, the user is ready to enable continuous tracking of the catheter. The physician can then move the catheter around outside the patient's body to determine if the registration is accurate enough to continue.

Although the registration from any single patient to a generic chest x-ray will obviously not be perfect in cases where a patient-specific chest x-ray is not available, the physician still can qualitatively make the decision whether the PICC line is placed correctly or incorrectly in most cases. If the registration from the patient to the generic image is very poor, then the physician has the option of either getting a chest x-ray of the patient, or simply inserting the PICC line the traditional way.
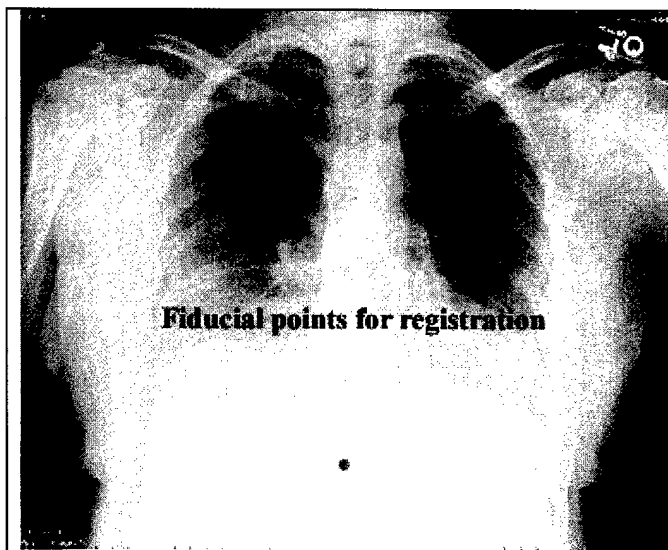
Figure 2: Fiducial points on a sample chest x-ray. The points correspond to the sternal notch, xiphoid process, and shoulder bones.

The physician is now able to begin inserting the catheter. The time it takes to do the pivot calibration and registration is actually very short. The entire process can be done in less than five minutes. With continuous tracking enabled, the catheter is displayed on the screen as a pointer which rotates to show the orientation of the tip. As the catheter is moved in the patient, the software continuously updates the position and orientation, showing the entire trail of the catheter path. If the screen becomes too cluttered, the user may click on a button to clear the screen and start displaying the pointers on a fresh image. The position of the catheter tip is shown in two dimensions in the plane of the x-ray. Since most of the motion of the catheter will be in that plane, and since the physician is already familiar with that view from the fluoroscope, we believe that this will be a good enough visualization for the procedure. The orientation angle is shown in three dimensions, with a visualization of the catheter going into or out of the screen when appropriate.

3. RESULTS

The software was evaluated qualitatively with a plastic model of a human torso to determine if the display would give a good enough visualization to be useful. The phantom consisted of a life-size plastic model of a human arm and chest with tubing to simulate the vasculature. The plastic 'veins' contained a junction of three different paths — down towards the heart, across the chest, and up towards the neck to simulate correct and wrong paths for the catheter. Six BB fiducials for registration were placed on the phantom and a chest x-ray was obtained of the model. Turns into wrong veins were easily seen in the display without any problem. In addition, we partially blocked a vein to simulate the catheter getting stuck, which was also detected immediately.

The graphical user interface for the program is shown in Figure 3. The steps in the planning and treatment process are indicated by the pushbuttons on the right hand side of the screen. The options for loading images and saving data are located in the pulldown menus at the top of the screen. The center-left shows the loaded x-ray image of our plastic torso phantom and is the main display window. The catheter pointer displays within the limits of this image window. The tip of the catheter is displayed as a magenta circle, with the orientation represented by light blue trailing lines. To create the catheter path display shown below, we threaded our catheter through the plastic tubing representing veins from the model's arm through to the chest.
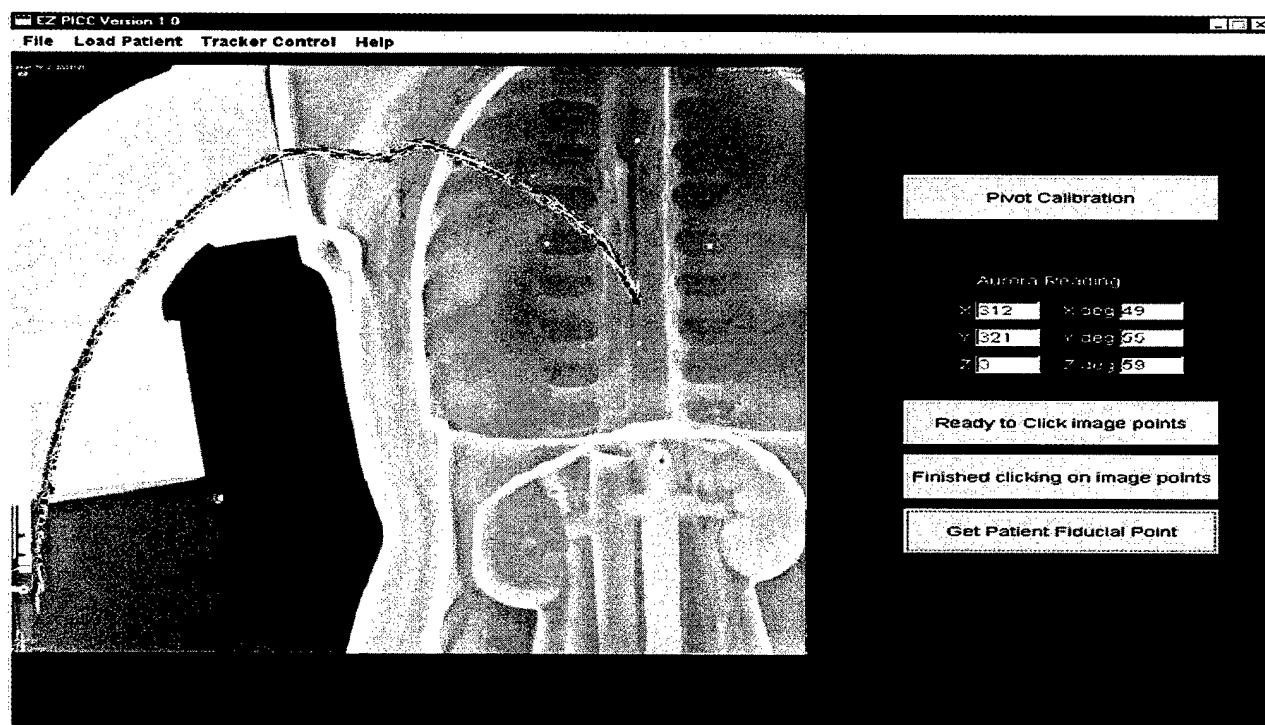
Figure 3: Graphical user interface with sample display of a catheter path.

The software was evaluated quantitatively for accuracy by the following method. We created an evenly spaced grid of nine points, and followed through the entire procedure for using our program. We first performed five pivot calibrations to determine the variability between trials. The variability was found to be negligible (< 0.2 mm). We then went through registration with all nine points and started continuous tracking. We defined the positional error of the system by the physical distance corresponding to the difference between where the pointer is displayed on the screen and the point on the image where it should actually be displayed. In other words, this corresponds to the difference between where the physician thinks the catheter is and where the catheter actually is in space. We calculated the orientation error by testing a set of eight angles (0, 45, 90...). We oriented the catheter at these angles and reported error as the difference between these and the measured angles of orientation. We feel that this gives a more useful assessment of the accuracy of the system than a simple registration error calculation. From five trials, we got an average positional error of 1.5±1.1 mm and an average orientation error of 2.6±1.3 degrees in the plane of the x-ray image. We believe that this accuracy is sufficient for the application.

4. DISCUSSION

As the reliability and quality of electromagnetic tracking systems increases, electromagnetic navigation has more potential for providing guidance in minimally invasive procedures. While some research groups have chosen to develop its application in more complex procedures such as cardiac arrhythmia surgery, we have chosen to research its feasibility in a more simple application. With this, we hope to show that electromagnetic tracking can easily be integrated into image-guided interventions. The Lucent Medical Systems Corporation developed a method for electromagnetically tracking PICC and CVC catheters in 1998. However, it differs from our research in several key points.

Their system consists of a small 1mm magnet implanted in the tip of a catheter, and a handheld display containing the magnet detectors. The handheld display is moved above the patient as the catheter is inserted, and the location of the catheter is displayed on a screen on the device (Figure 4). This system, however only shows the current location of the catheter tip, not the whole path history. Ours tracks the catheter more directly in 3D coordinates relative to the patient, while their system only gives the 2D location relative to the handheld sensor.

Figure 4: The Zortran detector developed by Lucent Medical Systems for catheter tracking (from www.lucentmedical.com/zortran.htm)

We have not taken the research to the next step of animal trials for the following reasons. A guidewire and catheter combination incorporating an electromagnetic fiducial was not available at the time of this work. In the real procedure a guidewire must first be placed independent of the catheter to establish the correct length of the catheter for each individual patient. In addition, even if we were to try this using a catheter alone to demonstrate the tracking concept, the current catheter is not steerable enough for such a procedure. The alternative electromagnetic navigation system described above has been successfully tested in pigs [3]. In addition, our research group has done similar work to use electromagnetic tracking in needle placement in swine and cadaver studies [5].

While we limited our research specifically to PICC line insertion, the software we have developed is general enough that it can be easily applied to other similar applications such as CVC placement, bronchoscopy, colonoscopy, and potentially any application where it would be useful to track the location of a catheter in the human body.

5. CONCLUSIONS

This paper presented a system to use an electromagnetic guidance system to track the catheter in PICC line placement. We believe that this type of system has broad applicability to other procedures and may become more widely used in the future. Optical tracking has already gained wide acceptance as a good method for tracking instruments outside the human body. Electromagnetic tracking provides a method that may be able to replace x-ray guidance in a wide variety of procedures. Our system could potentially be used at the bedside without real-time fluoroscopic guidance (only a final confirming x-ray would be needed) and free up fluoroscopy equipment for other procedures.

ACKNOWLEDGMENTS

REFERENCES

1. Worley SJ. "Use of a real-time three-dimensional magnetic navigation system for radiofrequency ablation of accessory pathways." *Pacing Clin Electrophysiol*, vol: 21(8), pp. 1636-45, Aug, 1998.

2. Zaaroor M, Bejerano Y, Weinfeld Z, Ben-Haim S. "Novel magnetic technology for intraoperative intracranial frameless navigation: in vivo and in vitro results." *Neurosurgery*, vol. 48(5), pp. 1100-7, May, 2001.

3. Gonzales, Andrei J. MD; Pestka, Cynthia BS; Silverstein, Fred MD; Golden, Robert N. PhD. "Peripherally inserted central catheter placement in swine using magnet detection." *Journal of Intravenous Nursing*. 22(3):144, May/June 1999.

4. Clifford MA, Banovac F, Levy E, Cleary K. "Assessment of hepatic motion secondary to respiration for computer assisted interventions." *Comput Aided Surg*, vol. 7(5), pp. 291-9, 2002.

5. Cleary K, Banovac F, Levy E, Tanaka D. "Development of a liver respiratory motion simulator to investigate magnetic tracking for abdominal interventions." Proc. SPIE Vol. 4681, p. 25-29, *Medical Imaging 2002: Visualization, Image-Guided Procedures, and Display*; Seong K. Mun; Ed., May 2002.

6. Glossop N, Banovac F, Levy E, Lindisch D, Cleary K, "Accuracy evaluation of the AURORA magnetic tracking system," poster presented at *Computer Assisted Radiology and Surgery (CARS)* conference, Berlin, Germany, June 2001.

10.6 Tang 2003: Breakdown of Tracking Accuracy ...

Reprint begins on the next page and is 6 pages.

Breakdown of Tracking Accuracy for Electromagnetically Guided Abdominal Interventions

Jonathan Tang*, Kevin Cleary *
*Imaging Science and Information Systems (ISIS) Center, Radiology Department, Georgetown University Medical Center, 2115 Wisconsin Ave., #603, Washington, DC
<jtang@isis.imac.georgetown.edu>

This study investigates the sources of error for an image-guided surgery system based on electromagnetic tracking. We characterized fiducial localization error in both magnetic and image space, modeled error propagation using a Monte Carlo simulation, and estimated system errors for registration schemes with minimal human error. Simulation results indicated that we would obtain much closer fiducial registration if we were to have a system with automatic fiducial localization.

1. INTRODUCTION

1.1 Purpose of Study

The purpose of this study was to investigate the error sources in an image-guided surgery system based on electromagnetic tracking that we been developing for minimally invasive abdominal interventions. This breakdown will enable us to better understand the effects of various components on the system accuracy.

Over the past two years, our research group has developed an image-guided surgery system [1] incorporating a beta version of the AURORA magnetic tracker (Northern Digital, Waterloo, Canada). In this system, registration is done based on pre-operative CT scans and a set of fiducials that can be localized in both image and magnetic space. The AURORA uses small sensor coils that can be embedded into the tip of needles or catheters to directly track their position and orientation. The system allows the physician to accurately guide a magnetically tracked needle into the abdominal area for a variety of interventional procedures that are usually done under x-ray fluoroscopy. The system has been tested on phantom torsos, respiratory motion simulators, and cadavers, all of which have been rigid-body approximations of true physiological conditions. In a liver phantom, the physician using the system has been able to target simulated liver tumors with successful placement in 14 of 16 attempts. However, the system does not perform as well with targets smaller than 1cm, deeper targets, and various other experimental conditions. This prompted us to investigate the error sources of the system.

The goals of this paper are:
- To characterize the overall fiducial localization error in both magnetic space and image space for our image-guided intervention system (IGS).
- To model error propagation in our IGS using a Monte Carlo simulation.
- To approximate the contribution of human error towards fiducial registration error and to simulate registration schemes without the influence of human error.

1.2 Registration Error Background

A common measure of overall fiducial misalignment is the root-mean-square error called *fiducial registration error* (FRE) [2]. The fiducial registration error is the number that most image-guided systems return after registration of coordinate systems. Fiducial misalignment stems from the inability to correctly determine fiducial locations in

magnetic space and image space. The determination of a precise point within a fiducial is called *fiducial localization*. The inevitable displacement of the localized point from the correct position is called the *fiducial localization error* (FLE). Such error occurs in both image and magnetic space. Misalignment of a target point due to registration is called Target Registration Error (TRE). For an in-depth mathematical review of FLE, FRE, and TRE, please consult [2].

2. METHODS

2.1 System Implementation

Figure 1 below shows the implementation of the system as recently used in a swine study in the interventional suite. The goal of this study was to hit simulated lesions in a swine liver using pre-procedure CT scans and image guidance based on electromagnetic tracking. The physician watches the image overlay shown in the lower left of the figure to manipulate the needle along a pre-planned path. Respiration is accounted for using another electromagnetically tracked needle (MagTrax, Traxtal Technologies, Bellaire, TX) that was placed in the liver prior to the CT scan. The current system had mixed success in accurately hitting the targets, which prompted us to investigate the sources of error described in this paper.

Figure 1 – Swine Study in the Interventional Suite

2.2 Error Breakdown

The main sources of FLE in our rigid model include errors in magnetic space, image space, and human error in physical space. The diagram below depicts the propagation of error from magnetic and image space to fiducial registration and target registration.
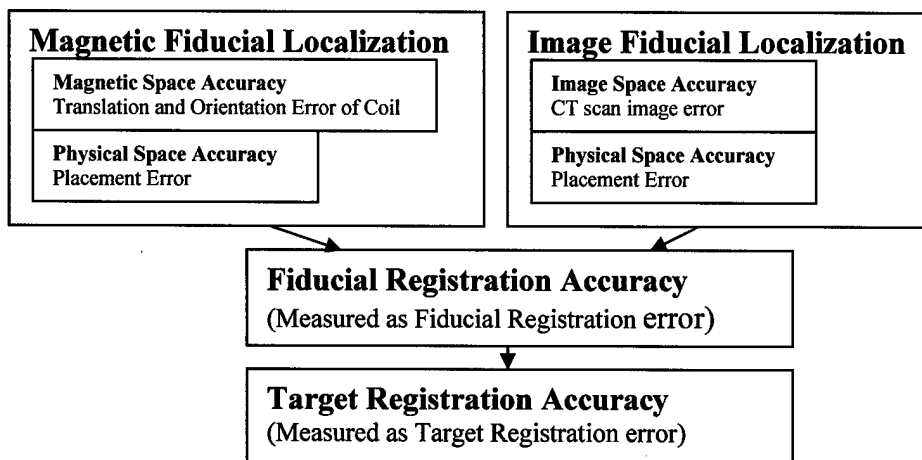
Magnetic Fiducial Localization	**Image Fiducial Localization**
Magnetic Space Accuracy Translation and Orientation Error of Coil	**Image Space Accuracy** CT scan image error
Physical Space Accuracy Placement Error	**Physical Space Accuracy** Placement Error

Fiducial Registration Accuracy
(Measured as Fiducial Registration error)

Target Registration Accuracy
(Measured as Target Registration error)

Figure 2 – Accuracy breakdown of our registration process

We categorized the error sources into three main groups: 1) magnetic space, 2) CT space, and 3) physical space.

1) **Magnetic space.** The most obvious error source is the inherent accuracy of the magnetic tracking system. We use circular multi-modality fiducials (IZI Corporation, Baltimore, MD) as skin fiducials in our registration process. For the experiment described in this paper, we built a custom plexiglass registration phantom using 0.8mm tantalum beads (Tilly Medical, Sweden) as fiducials. To localize a fiducial in magnetic space, the center of the fiducial is touched with a magnetically tracked probe. Error sources here include the placement error in manually localizing the center of the fiducial and error in calculating the location of the probe tip from the embedded sensor coil, which involves the combined translational and orientation error of the tracking system.

2) **CT space.** There will be some error inherent to the CT scanner and image reconstruction process but this is considered to be fairly small as we are using 1 mm slices in our experimental studies. Most of the error in localizing image fiducials will result from our manual process of choosing the center of the fiducials on the CT scan.

3) **Physical space.** In any registration procedure where manual intervention is required to select or localize the fiducials, there will always be human error. In our system, human error exists at the step where we localize the skin fiducials in magnetic space and image space; when the user taps out the centers of the skin fiducials on the patient and clicks on the center of the image fiducials on the CT scan. This error can not be directly measured independently from errors in the rest of our system. Errors in magnetic, image and physical space influenced the system's ability to accurately localize fiducials. These were considered fiducial localization errors (FLE) which contribute to fiducial registration accuracy (measured as fiducial registration error). From earlier work of Fitzpatrick et al. [2], we know that FLE is a contributor to targeting accuracy, measured as target registration error, along with the configuration and number of fiducials, and the distance of the target from the centroid of the fiducial configuration.

2.3 Measurement of Error

To better understand and quantify the contributions of some of these error sources, we conducted the following experiments:

- Experiment 1 examined the accuracy of the AURORA
- Experiment 2 investigated the offset from the coil position to the needle tip
- Experiment 3 measured fiducial localization error using a plexiglass phantom
- Experiment 4 modeled error propagation using a Monte Carlo simulation

Experiment 1: In previous work, the accuracy of the AURORA magnetic tracker was characterized in both translational and orientation aspects. In those experiments we used a novel six degree of freedom robot to serve as a precision positioning device. To measure positional accuracy, the robot was programmed to accurately place the magnetically tracked probe at 7 different positions over a 100x40x40mm volume [3]. For orientation accuracy, the robot was programmed to position the probe at the 8 corners of a 10x10x10mm volume, where the probe was oriented from -30 to 30 degrees in 10 degree increments [4]. The robot was considered accurate and ground truth from previous studies.

Results 1: Within the 100x40x40 mm volume, the AURORA was accurate to better than 1 mm [3] in translational position. The orientational study was done at the center of the AURORA workspace and found an orientation accuracy of better than 1 degree [4]. It should be noted that these were preliminary studies and a more definitive study with more trials and a larger workspace remains to be done.

Experiment 2: To measure the accuracy in calculating the position of the probe tip, we used the same robot and programmed it to pivot our magnetically tracked probe at its tip. Figure 3 below shows the robot holding the needle/probe for a pivot routine. This technique is the well known pivot routine that is used for calculating offsets between tracked sensors and the tip of the localization probe. From the position and orientation data collected, we were able to calculate the offset between the magnetic tracking coil and the tip of the probe. Using the offset, calculated in the least squares sense, we were able to determine the position of the tip given the position and orientation of the magnetic coil in the probe as returned by the AURORA system. The error in determining tip position was measured as the variance in the calculated tip position during several robot controlled pivot routines.
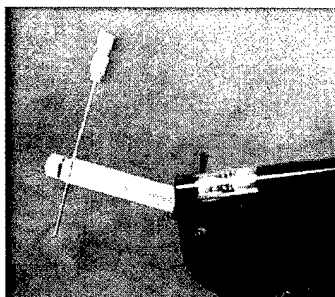
Results 2: The error in determining tip position was measured as standard deviations ranging from 0.2 mm to 0.5 mm depending on the speed of the pivot, the axis of rotation, and the needle used. We found that larger angle pivots done at slower speeds result in lower error.

Figure 3 - Robot doing pivot with sample needle

Experiment 3: To measure fiducial localization error in both magnetic and image spaces, we ran the registration procedure twenty-five times on our custom built plexiglass phantom, recording positions of both magnetic and image fiducials and the fiducial registration error. The phantom was constructed out of a 10x10x15cm solid block of plexiglass, where each side had five divot points with a 0.8mm tantalum bead embedded at each divot point. Four holes were drilled in the block to embed tracked needles used as internal fiducials.
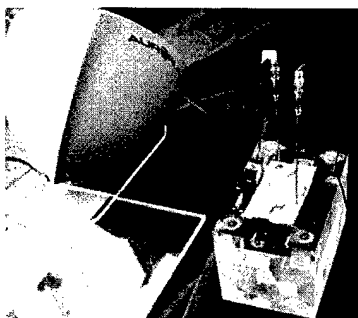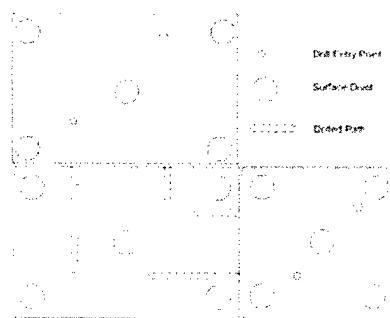

Figure 4 - Plexiglass phantom   **Figure 5 -Schematic of phantom**

In addition, we did fifteen trials of registration on our torso model using multi-modality skin fiducials, but found no statistically significant difference in registration results compared to using tantalum beads.

Results 3: We conducted twenty-five registration trials using this plexiglass phantom. The distributions of measured fiducials at each divot are best described as point clouds centered about fiducial position ground truth. The fiducial localization error was measured as the variance of each point cloud. The distribution of fiducials in magnetic space had a range of standard deviations between 0.23 and 2.24 mm with an average of 0.8mm. The distribution of fiducials in image space had a standard deviation of approximately 0.3 mm in the axial plane and 0.5mm between planes. We found that the average fiducial registration error for 25 manual registration trials was 1.1mm ranging between 0.7mm and 1.3mm with a standard deviation of 0.21mm. The internal fiducial, which was magnetically tracked and did not require any manual localization, had a very small standard deviation of 0.05mm.

Experiment 4: Using measurements of FLE from experiment 3, we modeled error propagation during the registration procedure with a Monte Carlo simulation done in Matlab. We assumed that the FLE of each fiducial is an independent identically distributed variable that can be modeled by a normal distribution with standard deviation 0.4mm for image fiducials and 0.8mm for magnetic fiducials. Using randomly perturbed fiducial locations, we calculated the best point-based rigid registration in the least squares sense. This calculation was done with 10 000 different perturbations as a Monte Carlo simulation. An example of the output is shown in Figure 7b. Using this simulation, we were able to estimate the effect of different FLE on the registration error.
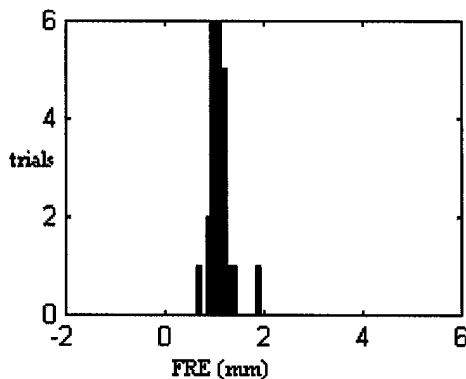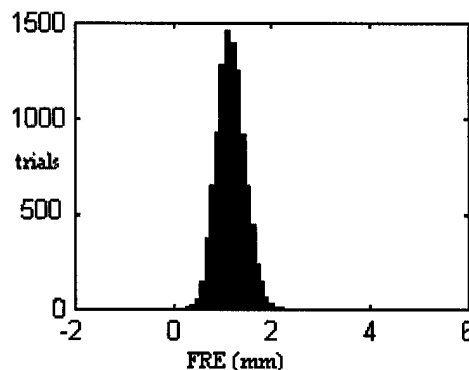

Figure 7a – experimental data   Figure 7b – simulation results

Results 4: During simulation trials, using 0.4mm as the standard deviation for image fiducial FLE, and 0.8mm as the standard deviation for magnetic fiducial FLE, we find the average of FRE to be 1.17 +/- 0.28mm. (Figure 7b) This is consistent with experimental data (1.1 +/- 0.21mm) from twenty-five trials done in experiment 3. (Figure 7a) To simulate computerized selection of image fiducials, we used 0.0mm as the standard deviation for image fiducial FLE, and 0.8mm for magnetic fiducials. We chose to use a standard deviation of 0.0mm for image fiducials because computerized selection of fiducials results in the same coordinates every time. For that simulation, we get a registration error of 1.0 +/- 0.25mm. To estimate the registration error when the procedure has an automatic localization process, we changed the parameters of the

simulation such that it would calculate registration with FLE equal to the internal tracked fiducial (~ 0.05mm). This effectively simulates automatic localization of skin fiducials as if they were magnetically tracked fiducials on the skin surface. Registration error was predicted to be 0.54 +/- 0.13mm. This shows that we can reduce most of the registration error if we automatically localize our skin fiducials.

3. CONCLUSION

There are many factors that can contribute to the overall accuracy of an image-guided surgery system based on magnetic tracking. A systematic analysis is necessary to isolate critical factors and determine how optimal performance can be achieved. We believe that the greatest contributor to registration error is from the manual fiducial localization process. Our simulation indicated that if we were to have a system with automatic fiducial localization, we would obtain much closer fiducial registration.

ACKNOWLEDGMENTS

REFERENCES

1. Banovac F, Glossop N, Lindisch D, Tanaka D, Levy E, Cleary K, "Liver tumor biopsy in a respiring phantom with the assistance of a novel electromagnetic navigation device", 5th International Conference on Medical Image Computing and Computer Assisted Intervention, Springer, pages 200-207, Sept. 2002.
2. Fitzpatrick J. M., West J. B., Maurer C.R. Jr, "Predicting Error in Rigid-Body Point-Based Registration", IEEE Transactions on Medical Imaging, pages 694-702, Vol. 17 No. 5 Oct 1998.
3. Banovac F, Glossop N, Jay M, Lindisch D, Cleary K, "Feasibility of image-guided abdominal interventions using a novel magnetic position sensing device in an interventional radiology suite," *Computer Assisted Radiology and Surgery (CARS)*, page 1091, June 2002.
4. Corral G., Cleary K, Tang J, Levy E, Glossop N, "Orientation Accuracy of a Magnetic Tracking device in Image-Guided Intervention", *Computer Assisted Radiology and Surgery (CARS)*, June 2003, this volume.

10.7 Tang 2004: Respiratory Motion Tracking ...

Reprint begins on the next page and is 6 pages.

Respiratory Motion Tracking of Skin and Liver in Swine for CyberKnife Motion Compensation

Jonathan Tang[a][*], Sonja Dieterich[b], Kevin Cleary[a]

[a]Imaging Science and Information Systems (ISIS) Center, Georgetown University
2115 Wisconsin Ave NW, Suite 603, Washington DC, 20007 USA
[b]Department of Radiation Oncology, Georgetown University Hospital/ Medstar Health
3800 Reservoir Road, Washington DC, 20007 USA.

1. ABSTRACT

In this study, we collected respiratory motion data of external skin markers and internal liver fiducials from several swine. The POLARIS infrared tracking system was used for recording reflective markers placed on the swine's abdomen. The AURORA electromagnetic tracking system was used for recording 2 tracked needles implanted into the liver. This data will be used to develop correlation models between external skin movement and internal organ movement, which is the first step towards the ability to compensate for respiratory movement of the lesion. We are also developing a motion simulator for validation of our model and dose verification of mobile lesions in the CYBERKNIFE Suite. We believe that this research could provide significant information towards the development of precise radiation treatment of mobile target volumes.

Keywords: Respiratory Motion Tracking, Cyberknife

2. PURPOSE

Radiation treatment of mobile lesions has been a long standing challenge in radiation therapy. The ability to compensate for respiratory motion of internal organs is highly desirable in stereotactic radiosurgery. Previous researchers have shown that it may be possible to predict internal organ motion using external skin marker information.[1] The purpose of this study was to collect respiratory motion data of skin markers and internal fiducials from several swine studies. We hope to use this data to implement and evaluate a correlation algorithm between external skin motion and internal organ motion. We are also developing a motion simulator device to reproduce these respiratory motions for evaluation of the correlation model. This motion simulator can also be used for dose verification of mobile lesions. Our research goal is to develop methods for precise radiation treatment of mobile target volumes.

3. METHODS

The CYBERKNIFE (Accuray, Sunnyvale CA) is a radiation treatment system that incorporates a linear accelerator mounted on a robotic arm (Figure 1). It is able to track tumor location using two orthogonal x-ray cameras that track fiducials inserted before radiation treatment. The system, as currently installed at Georgetown University Hospital, can automatically compensate for up to 10 mm of patient movement but only once every 30 to 60 seconds. Since robotic control of the linear accelerator provides the unique possibility to do real-time tumor motion tracking during stereotactic radiosurgery, Accuray has developed SYNCHRONY, a real-time tracking system that aims to precisely track lesions in organs with significant respiratory motion. With SYNCHRONY, a correlation model between skin motion and internal organ motion is established by tracking skin motion with infrared markers and tracking implanted fiducials with two orthogonal x-ray cameras. The CYBERKNIFE robotic arm follows the internal organ motion based on the prediction from the skin motion. To validate this technology, there exists a need for external and internal respiratory motion data obtained at fast rates and a motion simulator platform to replicate the respiratory motion.

---

*Contact information: Jonathan Tang jtang@isis.imac.georgetown.edu, phone (202)-687-2902
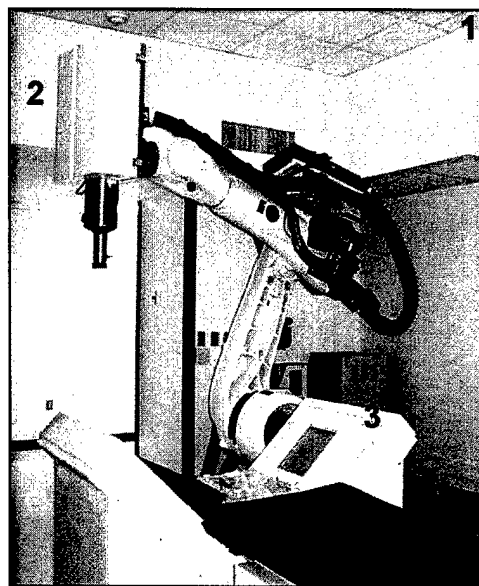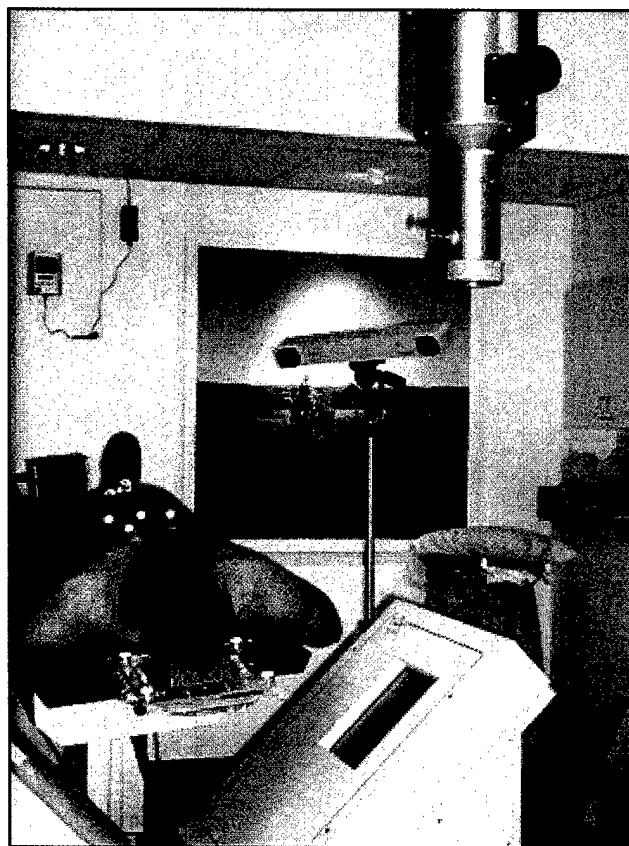
Figure 1: (top) CyberKnife Suite at Georgetown University Hospital

Figure 2: (left) Skin Motion Tracking with the POLARIS in the CYBERKNIFE Suite.
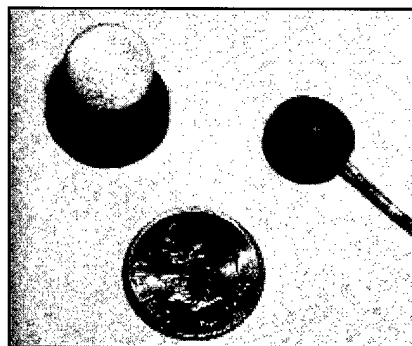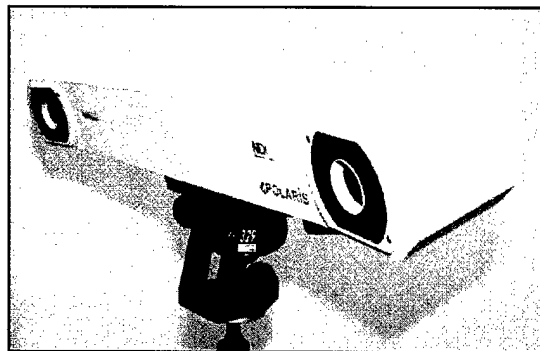

Figure 3a: (left) Polaris Optical Tracking System.
Figure 3b: (right) Polaris Passive and Active Marker

Previously our group has shown the feasibility of fast update tracking of external fiducials in the CYBERKNIFE suite[2] (Figure 2, Figure 3ab). Using the POLARIS optical tracker (Northern Digital Inc, Waterloo, Canada), we tracked four reflective skin makers placed on patients' chests during radiosurgery treatment in the CYBERKNIFE suite under an IRB approved protocol. That data has proven useful in studying external skin motion of human patients, but does not provide information about the movement of internal fiducials. In this paper, we collected positions of both external and internal fiducials in swine to provide data for respiratory motion compensation research.
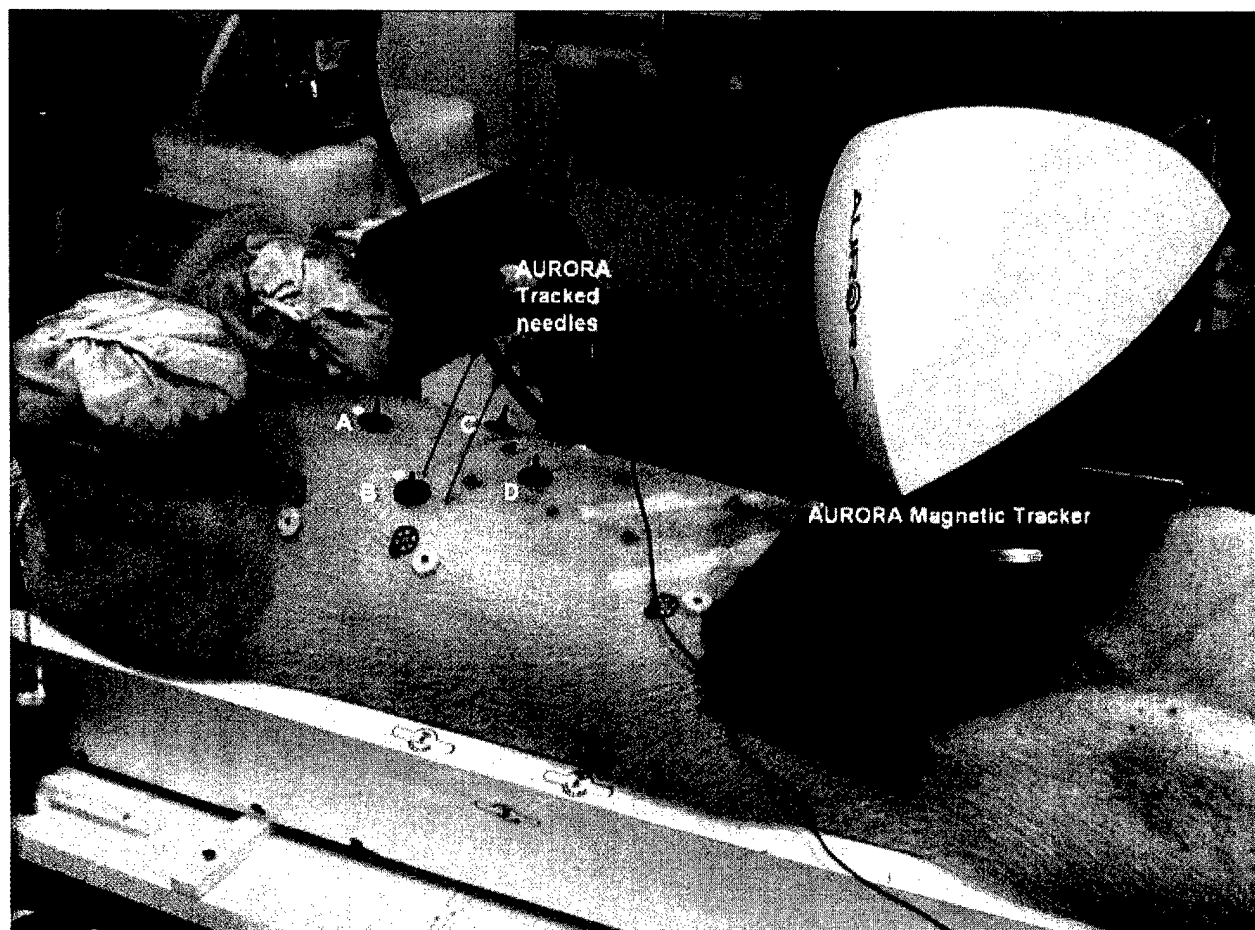
Figure 5 - Tracking of Internal fiducials and External skin markers in swine

We obtained approval from the Georgetown Animal Care and Use Committee to track external and internal fiducials in four swine. The POLARIS infrared tracking system was used for recording 4 passive reflective markers placed on the swine's abdomen. The AURORA electromagnetic tracking system (Northern Digital) was used for recording 2 electromagnetically tracked needles (Traxtal Technologies, Bellaire, Texas) implanted into the liver. The AURORA field generator, the 2 needles, and the 4 passive markers are shown in Figure 5.

In order to register the AURORA to the POLARIS coordinate system, we localized the position of the POLARIS optically tracked skin markers with the AURORA tracked needles by removing the reflective sphere ball and pointing to the plastic stem presumed to be in the center of the reflective sphere. We can solve for the transformation matrix that registers both coordinate systems, given the positions of the four markers in both POLARIS and AURORA space.

Fiducial location data was recorded at 10 hertz for external skin marker data, and 30 hertz for internal fiducial data, for a duration of four minutes with the swine ventilated at twelve breaths per minute.

4. RESULTS

The first two columns of Table 1 show the position of the skin fiducials localized in both POLARIS and AURORA coordinate systems. This data was taken from the most recent swine study, and has been rounded to the first decimal place. Column 1 lists the skin markers as measured with the POLARIS tracker, column 2 lists the same skin markers as measured by the AURORA tracker. We registered the two coordinate systems together and applied the resulting frame transformation to the skin markers measured in AURORA coordinate space. Column 3 is the result of

transforming the skin markers from AURORA to POLARIS coordinate space. The transformation matrix can be used
to transform any coordinate measured in AURORA space into corresponding POLARIS space.

Table 1: Position of Skin Fiducials From Most Recent Study (distances in mm)

	Skin Markers (POLARIS space)	Skin Markers (AURORA space)	Transformed Skin Markers (AURORA to POLARIS space)
A.	338.8, 56.6, -1467.8	-109.9, 112.8, -216.8	338.4, 57.6, -1464.4
B.	363.5, -1.7, -1424.4	-61.1, 120.3, -156.2	365.1, -1.5, -1420.7
C.	339.8 13.8 -1511.6	-100.3, 42.7, -214.8	338.9, 15.0, -1520.9
D.	352.3, -36.9, -1477.2	-65.5, 53.1, -152.2	352.0, -39.4, -1475

The registration error for this transformation was 5.7mm. Registration error is calculated as the root mean square error
between transformed AURORA fiducial positions and POLARIS fiducial positions. Figure 6 shows the first ten
seconds of data from one external and one internal fiducial. Frequency analysis indicates that internal and external
fiducial movement is in phase with the largest frequency component between 0.18 and 0.21 hertz (equivalent to 11 to
12.5 breaths per minute) as shown in the FFT analysis of the POLARIS data in Figure 7.
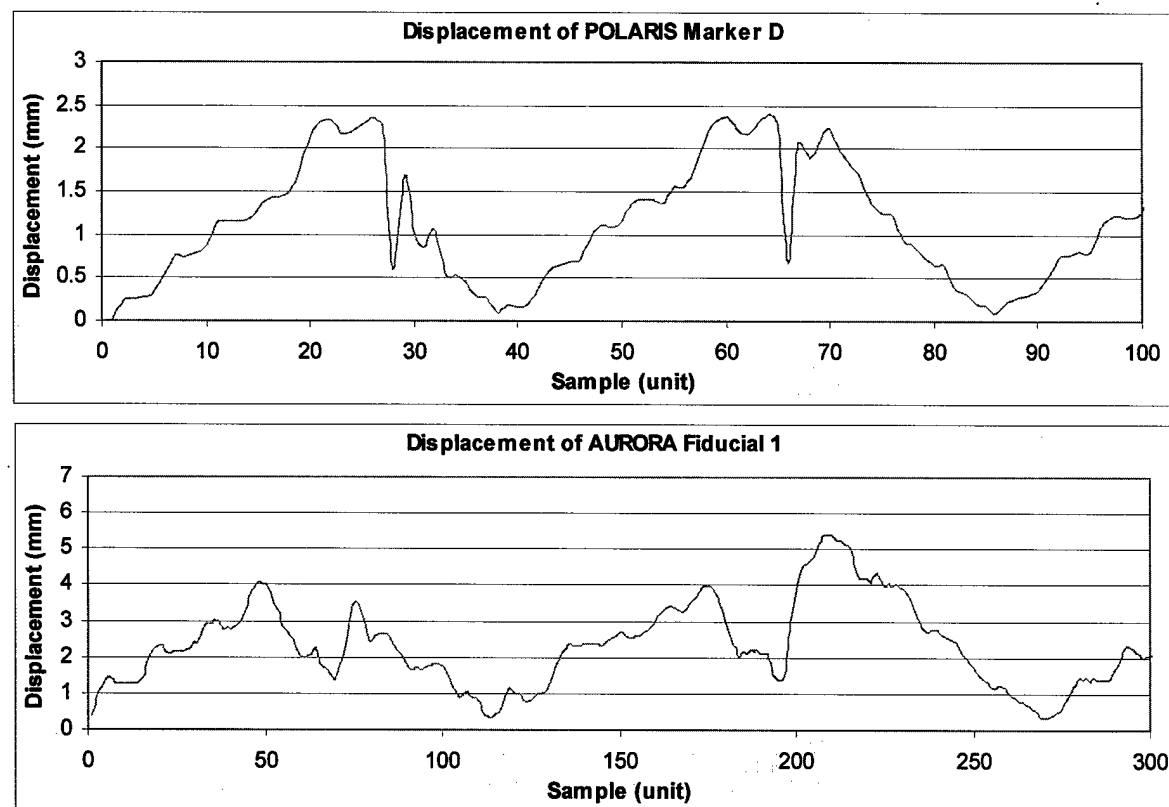
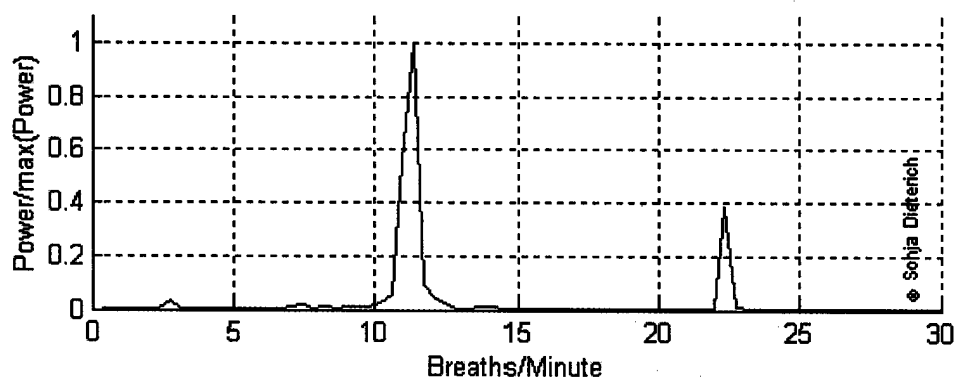**Figure 6: Ten seconds of respiratory motion for both external and internal fiducials.**

Figure 7 - Skin motion FFT showing main frequency component at 11 breaths / minute.

The data from these animal studies was used to program a respiratory motion simulator customized for the CYBERKNIFE Suite at Georgetown University Hospital. The respiratory motion simulator consists of two independent and programmable three-dimensional motion platforms built completely with off-the-shelf components. (Figure 8ab) Wiring, assembly and software development were done in-house at Georgetown University. The components were selected based on the technical requirements of motion amplitude and frequency, which were established from real patient data taken at Georgetown University Hospital. The platforms are controlled by a PC through an Ethernet-addressable motion control board. (Galil Motion Control, Inc.) See Figure 8a for a picture of the respiratory motion simulator in the CYBERKNIFE Suite.

The simulator is able to precisely simulate the three-dimensional respiratory motion of skin and internal organ fiducial markers. This motion simulator, along with external and internal fiducial motion gathered from animals in this study, will be used to assist in implementing and evaluating correlation algorithms between external skin motion and internal organ motion. This motion simulator can also be used for dose verification of mobile lesions in the CYBERKNIFE Suite.
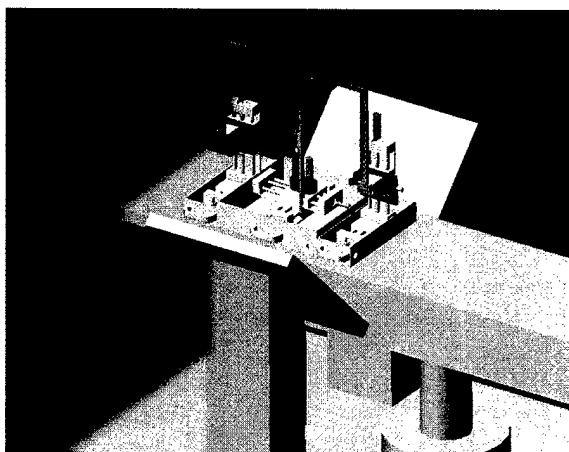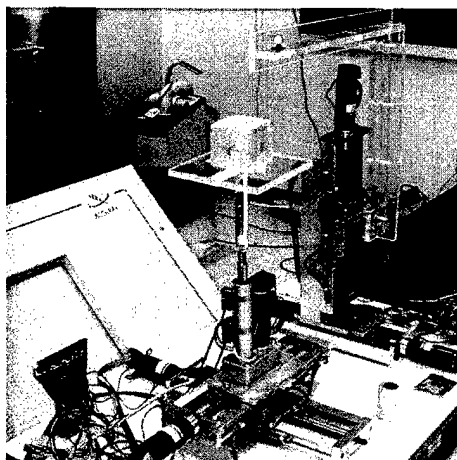

Figure 8ab - Motion Simulator for Cyberknife Suite on table (left) and 3D Model (right)

5. CONCLUSION

In this study, we have collected respiratory motion data from several swine using the POLARIS optical tracker and AURORA magnetic tracker. This will be used to develop correlation models between external skin movement and internal organ movement, which is the first step towards the ability to compensate for respiratory movement of the lesion. We are also developing a motion simulator for validation of our model and dose verification of mobile lesions in the CYBERKNIFE Suite. We believe that this research could provide significant information towards the development of precise radiation treatment of mobile target volumes, which is an extremely important clinical problem.

6. ACKNOWLEDGMENTS

7. REFERENCES

1. Schweikard, A., Glosser, G., Bodduluri, M., Murphy, M., Adler, J. R., Robotic Motion Compensation for Respiratory Motion during Radiosurgery, *J. Computer Aided Surgery, 5, 4, 263-277, Sept. 2000.*

2. Dieterich S., Tang J., Rodgers J., Cleary K., Skin Respiratory Motion Tracking for Stereotactic Radiosurgery using the Cyberknife, *Computer Assisted Radiology and Surgery* Elsevier, Volume ICS 1256, 130-136, 2003, London UK.

10.8 Xu 2003: Registration and Tracking

Reprint begins on the next page and is 9 pages.

3D motion tracking of pulmonary lesions using CT fluoroscopy images for robotically assisted lung biopsy

Sheng Xu[a], Gabor Fichtinger[a], Russell H. Taylor[a], Kevin Cleary[b]

[a]Engineering Research Center, Johns Hopkins University, Baltimore, MD, USA 21218;
[b]Imaging Science and Information Systems (ISIS) Center, Department of Radiology, Georgetown University Medical Center, Washington DC, USA 20007

ABSTRACT

We are developing a prototype system for robotically assisted lung biopsy. For directing the robot in biopsy needle placement, we propose a non-invasive algorithm to track the 3D position of the target lesion using 2D CT fluoroscopy image sequences. A small region of the CT fluoroscopy image is registered to a corresponding region in a pre-operative CT volume to infer the position of the target lesion with respect to the imaging plane. The registration is implemented in a coarse to fine fashion. The local deformation between the two regions is modeled by an affine transformation. The sum-of-squared-differences (SSD) between the two regions is minimized using the Levenberg-Marquardt method. Multi-resolution and multi-start strategies are used to avoid local minima. As a result, multiple candidate transformations between the two regions are obtained, from which the true transformation is selected by similarity voting. The true transformation of each frame of the CT fluoroscopy image is then incorporated into a Kalman filter to predict the lesion's position for the next frame. Tests were completed to evaluate the performance of the algorithm using a respiratory motion simulator and a swine animal study.

Keywords: motion estimation, real-time tracking, robust tracking, data association, textured regions, lung biopsy, robotics

1. INTRODUCTION

In lung biopsy, the position of the target lesion may vary due to intrinsic causes such as respiratory motion or extrinsic reasons such as interactions between the tissue and a surgical tool. In developing a robotic system to assist in biopsy, we need to provide some way to track the target lesion. CT fluoroscopy combines the advantages of both CT and fluoroscopy, which offers an opportunity to track the motion of the target lesion in real-time during the intervention. Our prototype system is shown in Fig. 1. The real-time CT fluoroscopy image is captured using a frame grabber (Accustream 170, Foresight Imaging, Lowell, Massachusetts, USA). The position of the target lesion is detected from the image,
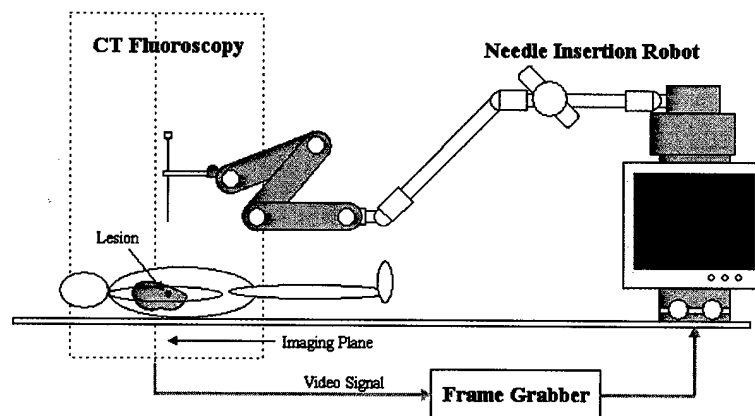

Fig. 1 CT fluoroscopy guided robotically assisted lung biopsy

which serves as input for the robot controller to compensate for the motion. This paper presents a motion analysis method to estimate the 3D motion of a target lesion using the CT fluoroscopy image sequences. The method aims at tracking the lesion's motion no matter whether the lesion is inside or outside the imaging plane.

Motion tracking is a well-established area of research in computer vision. The tracking methods can be broadly classified into feature-based and region-based approaches. The feature-based approaches rely on the extraction of a sparse set of image primitives corresponding to distinctive scene features and the matching of such features over time using some form of search procedure. The type of features can be points, lines, edges, corners or contours. It is required for these approaches that the features being tracked stay in the scene. For the purpose of tracking pulmonary lesions using CT fluoroscopy, the available features in the CT fluoroscopy image are blood vessels and bronchi. Due to respiratory motion, the features specified in one frame may not be in another frame. Therefore, the feature-based approaches cannot be applied.

The region-based approaches make direct and complete use of all available image intensity information, therefore eliminating the need to identify and model a special set of features to track. The tracking algorithm of this paper falls into this category. The algorithm minimizes the sum-of-squared differences (SSD) between two regions. Variants of this method have been presented in previous work by other researchers. For example, Rehg and Witkin [1] tracked affine deformations; Hager and Belhumeur [2] reformulated the tracker for real-time performance; Shi and Tomasi [3] connected images texture, numerical issues, and tracker performance; Szeliski and Coughlan [4] used the Levenberg-Marquardt method as a problem solver to track multi-bilinear patches; and Gleicher [5] introduced difference decomposition to solve the registration problem in tracking, where the difference was a linear combination of a set of basis vectors.

The goal of this tracking algorithm is to guide a surgical-assist system (a needle placement robot). Therefore, the algorithm must be robust to be clinically acceptable. In the existing literatures on robust tracking, Toyama and Hager [6] presented the "Incremental Focus of Attention" architecture, which switches between algorithms according to the visual environment to achieve robust performance. McCane et. al [7] presented a framework for merging the results of independent motion trackers using a classification approach. Chen et. al [8] used neighborhood relaxation with multi-candidate pre-screening to robustly track image regions.

2. METHODS

Using CT fluoroscopy, the anatomy in the imaging plane can be viewed in real-time. Although the target lesion may not always stay in the imaging plane due to respiratory motion, the location of the target lesion with respect to the imaging plane can be estimated from a pre-operative CT volume. As shown in Fig. 2, a small region A is initially selected by the physician in the pre-operative image such that the region is close to the target lesion and has rich texture. If this region and the target lesion are close enough, they will have approximately the same deformation. By registering the region A to its corresponding region B of the pre-operative CT volume, the location of the target lesion with respect to the imaging plane can be estimated using the local rigidity around the lesion. The framework of the algorithm is shown in Fig. 3. The position of the current CT fluoroscopy region in the CT volume is predicted from previous frames. The CT

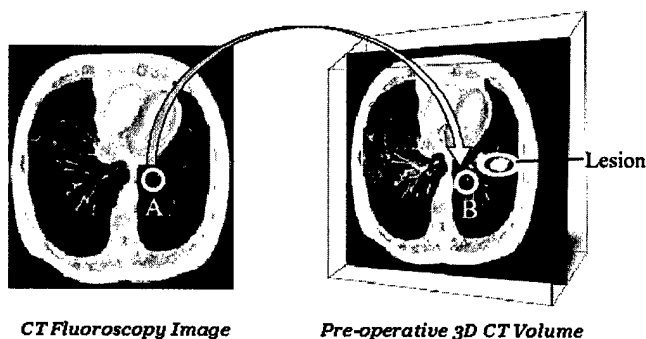CT Fluoroscopy Image   Pre-operative 3D CT Volume
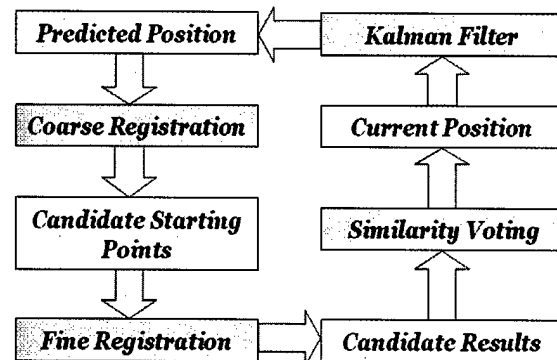
Fig.2 Local registration

Fig.3 Algorithm framework

fluoroscopy image region is then registered to the CT volume in a coarse-to-fine fashion. A multi-start strategy is used during the process, so multiple results are generated. The true motion of the CT fluoroscopy region is selected from these candidate results by similarity voting. The selected motion vector is then incorporated into a Kalman filter to predict the region's position for the next frame.

2.1 Coarse registration

The purpose of the coarse registration is to find good starting points for the fine registration. It is necessary that at least one of these starting points will lead to the solution of the fine registration. Since the CT fluoroscopy image has a large slice thickness (10 mm in our case), the CT volume is resampled to the same slice thickness. The original slice interval is preserved. Although the adjacent two slices have overlap in the resampled CT volume, it doesn't change the spatial position of each slice. Each slice of the resampled CT volume is then downsampled to a lower resolution. The sample rate is determined by the size of the convergence region of the fine registration so that at least one sampled pixel will fall inside the basin surrounding the minimum of the SSD residual. Cross correlation is performed at the pixel level to estimate the relationship between the CT fluoroscopy image region and the CT volume. The pixels best correlated with the center of the CT fluoroscopy image region are selected to be the starting points of the fine registration.

2.2 Fine registration

The lung has rich textures formed by blood vessels and bronchi, which allows the use of local information to register the CT fluoroscopy image region to the CT volume. As shown in Fig. 2, by registering the tissue inside the region to the pre-operative CT volume, the location of the target lesion with respect to the imaging plane can be determined using the local rigidity around the lesion in the CT volume. The shape of the region can be either a ring or a disk in this research, depending on which shape encloses more texture in the CT fluoroscopy image. The advantage of using a circular region is that it better approximates the motion of the region with respect to its surrounding area. Before the registration, the CT volume is smoothed by Gaussian filters. Gradient images are then calculated. The tracking algorithm is based on minimizing the SSD between the selected region in the CT fluoroscopy image and a corresponding one in the CT volume. The Levenberg-Marquardt method [9] is used to solve the SSD objective function with a good starting point. Compared to other methods for solving least square problems, the Levenberg-Marquardt method is more robust, which usually results in a larger convergence region.

The CT fluoroscopy image usually has a large slice thickness. As shown in Fig. 4, the 2D CT fluoroscopy image is actually the projection of all the tissue inside the dashed box on the imaging plane. As a result, the CT fluoroscopy image cannot be registered to the preoperative CT volume directly. What can be done is to find a subvolume of the preoperative CT volume corresponding to the dashed box, and then stack the tissue of the subvolume together to generate a synthetic CT fluoroscopy image. If the real and the synthetic CT fluoroscopy images match each other, the registration is done. The following equation (1) describes the relationship between the 2D CT fluoroscopy image I and its corresponding 3D
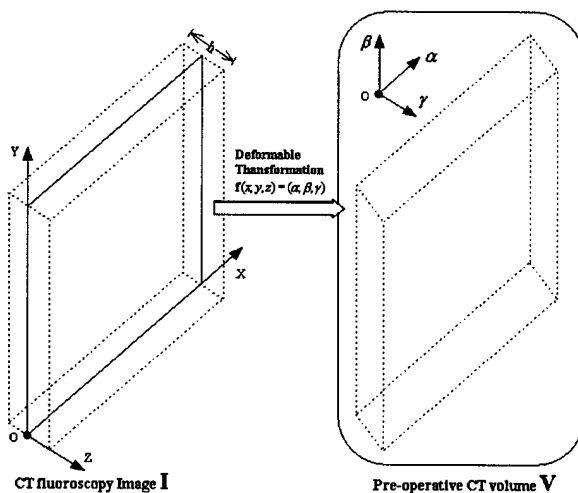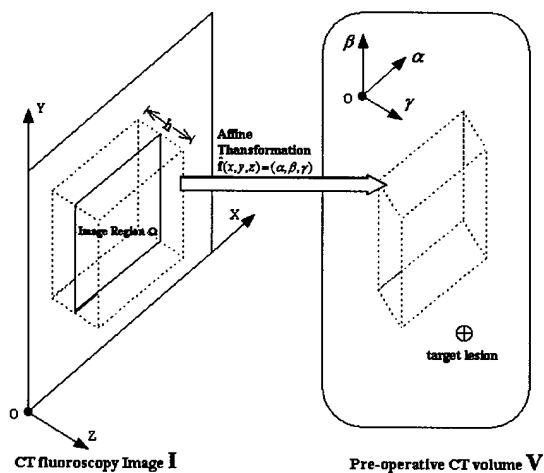

Fig.4 CT fluoroscopy image and CT volume

Fig.5 Local registration

subvolume V in preoperative CT:

$$\mathbf{I}(x, y) = \frac{1}{h} \int_{z=-h/2}^{h/2} \mathbf{V}(\ \mathbf{f}(x, y, z)\ )dz + \mathbf{n}(x, y) \tag{1}$$

where $\mathbf{n}$ represents the noise, $\mathbf{f}$ represents a deformable transformation and h is the slice thickness of the CT fluoroscopy image. The integral is to project the subvolume on a plane to simulate the CT fluoroscopy image. It can be realized by tri-linear interpolation.

The deformation of the lung tissue can be very complicated. However, if the region to be registered is small, the deformation can be approximated using 3D affine transformation, which is a 3 by 4 parameter matrix represented by $\hat{\mathbf{f}}$ in Fig. 5. Equation (2) shows a basic objective function to be minimized. It is a weighted SSD between the CT fluoroscopy region and the synthetic region.

$$O(\boldsymbol{\mu}) = \sum_{(x,y)\in\Omega} w_a^2 w_b^2 \left[\frac{1}{h} \int_{z=-h/2}^{h/2} \mathbf{V}(\ \hat{\mathbf{f}}(x, y, z, \boldsymbol{\mu})\ )dz - \mathbf{I}(x, y) \right] \tag{2}$$

where $\boldsymbol{\mu}$ is a vector of twelve parameters of the affine transformation to be estimated; w_a is a Gaussian window function which gives the central pixels a larger weight. As a result, the outer pixels that can not be well represented by the affine transformation will not have a large effect on the objective function. w_b is another weighting function with gives the brighter pixels a larger weight as described in Equation 3.

$$w_b = \max \left[\frac{1}{h} \int_{z=-h/2}^{h/2} \mathbf{V}(\ \hat{\mathbf{f}}(x, y, z, \boldsymbol{\mu})\ )dz, \quad \mathbf{I}(x, y) \right] \tag{3}$$

The purpose of w_b is to emphasize the bright texture generated by the blood vessels and bronchi. If both of the pixels being compared are dark, their effect on the objective function will be minimal. The dark pixels usually correspond to the parenchyma of the lung, which can only generate noise to the SSD.

Normally, SSD is only used for the intra-modality registration. It can be shown that SSD is the optimum measure when two images only differ by Gaussian noise [10]. In this tracking problem, the image regions being compared come from the same machine but two different imaging methods – the standard CT and the CT fluoroscopy, which results in an intensity difference between the two regions. If this intensity difference is big, SSD misregistration will happen. Although there is no simple relationship to map the intensity from one imaging method to the other, the effect of the intensity difference can be reduced by subtracting the mean of the intensity from both regions. The revised objective function is then the following:

$$O(\boldsymbol{\mu}) = \sum_{(x,y)\in\Omega} w_a^2 w_b^2 \left\{ \left[\frac{1}{h} \int_{z=-h/2}^{h/2} \mathbf{V}(\ \hat{\mathbf{f}}(x, y, z, \boldsymbol{\mu})\ )dz - C_V \right] - \left[\mathbf{I}(x, y) - C_I \right] \right\} \tag{4}$$

where C_v and C_I are the intensity means of the synthetic region and the CT fluoroscopy region respectively. They are given in equations 5 and 6, in which N is the number of pixels inside the region of interest Ω.

$$C_v = \frac{1}{N} \sum_{(x,y)\in\Omega} \frac{1}{h} \int_{z=-h/2}^{h/2} \mathbf{V}(\ \hat{\mathbf{f}}(x, y, z, \boldsymbol{\mu})\ )dz \tag{5}$$

$$C_I = \frac{1}{N} \sum_{(x,y)\in\Omega} \mathbf{I}(x, y) \tag{6}$$

Technically, the mean of the synthetic region is a function of the unknowns of the affine transformation. However, the SSD function is solved iteratively. Since the step size is very small between two consecutive iterations, the change of mean is tiny and has little effect on the solution. Therefore, the intensity mean of the synthetic region is treated as a

constant. It was found that the subtraction of the mean intensity from the original intensity is very effective in improving the robustness of the algorithm.

The reason to use SSD is to replace the image registration problem with non-linear minimization. Using the standard optimization methods, the tracking algorithm can be very efficient. There is no need to evaluate the entire objective function to calculate its derivatives. The derivatives can be obtained from the image gradients calculated offline from the pre-operative CT volume.

2.3 Similarity voting

Both multi-start and importance sampling strategies are used to avoid local minima, which result in multiple candidate transformations of the CT fluoroscopy image region. Many of these transformations are false results caused by local minima of the SSD residual error. Even if the global minimum is found, it may not be the true transformation due to the effect of the image noise. In response to these problems, similarity voting is used to distinguish the true transformation from the false transformations. The following measures are used to evaluate the similarity between the CT fluoroscopy image region and the synthetic region.

- a) Residual error of the pixels inside the region
- b) Residual error of the pixels surrounding the region
- c) Residual error of the bright pixels inside the region
- d) Axis orthogonality

In the above similarity measures, (a) is the value of the SSD objective function and (b) gives the "global" information of the region. The bright pixels in (c) are segmented using automatic thresholding [11]. They are emphasized because the blood vessels and bronchi appear bright in the image, which form most of the useful texture. The assumption for (d) is that the deformation is small, so the principle axes are nearly perpendicular to each other after the affine transformation. Although none of the four similarity measures is sufficient to independently determine the true transformation, the true transformation should generally have larger values of the similarity measures compared to the other candidate transformations. If the candidate transformations are ranked in terms of overall evaluations from all the similarity measures, the true transformation is very likely to have the best overall ranking. As shown in Fig. 6, the candidate transformations are evaluated and ranked for each similarity measure. The four rankings for each candidate are summed. The candidate transformation with the smallest sum is selected. With enough similarity measures, the similarity voting can be robust in picking out the true motion vector. In addition, it avoids using arbitrarily set thresholds, which is problem specific and prone to failure.

2.4 Kalman filtering

The Kalman filter is a classical tool that produces estimates optimal in the least-squares sense of the state of a dynamic system from noisy measurements and an uncertain model of the system dynamics. The use of predictors like Kalman filter can reduce computational cost by only processing a certain area of the image, and the noise outside that area does not influence the processing [12]. The price paid for the efficiency is the increased possibility of dropping the true motion vector. Using the multi-start strategy mentioned above, the dropping problem can be alleviated. In this research, the dynamic system equation of the Kalman filter is chosen to be a constant velocity update. Although it is possible to
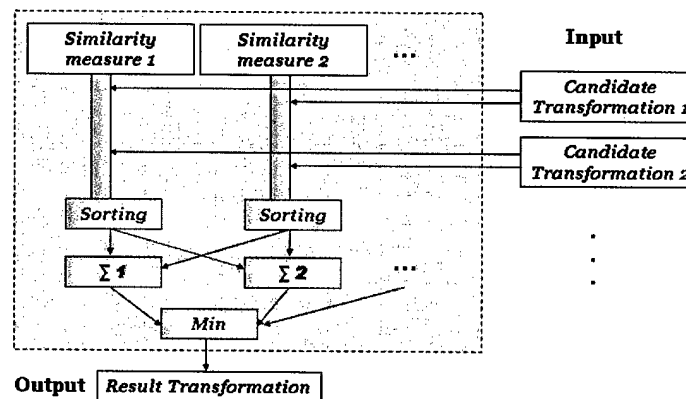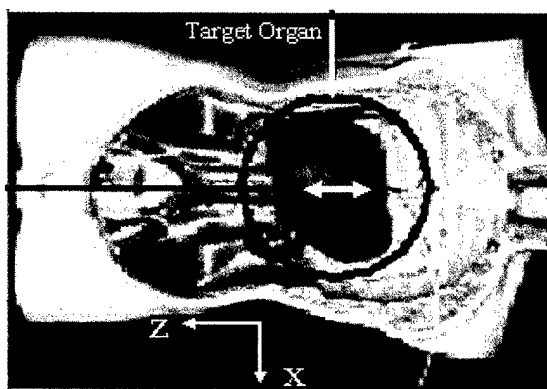

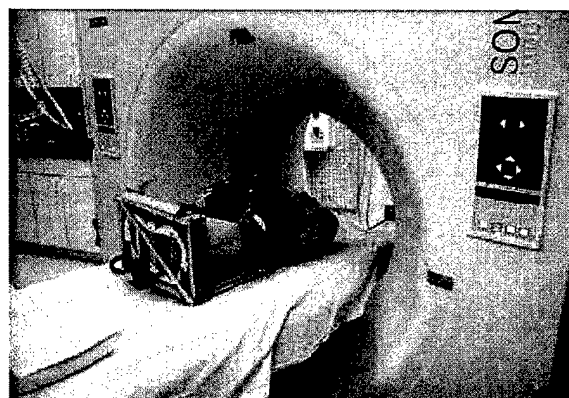Fig.6 Similarity voting

Fig.7 Respiratory motion simulator

Fig.8 Motion tracking test of respiratory motion simulator

use a more complicated motion model to boost the Kalman filter's performance, the disadvantage is that the tuned Kalman filter is effective only for a narrow class of motions. Given that the motion of the target lesion is not limited to respiratory motion, and the patient can hold the breath during the needle insertion, it may not be worthwhile to employ a complicated motion model.

3. EXPERIMENTAL RESULTS

Three experiments were carried out using both synthetic and real CT fluoroscopy images (Siemens Somatom Volume Zoom CT). The synthetic CT fluoroscopy image was generated from a pre-operative CT volume of the lung region with 2.0 mm slice thickness and 0.72 mm pixel size. As a result, the exact match of the CT fluoroscopy image region is known. Clustering analysis of the SSD objective function was performed. It was observed that, for the objective function to converge, the starting point had to be within ±2mm for translation and within ±20° for each of the three rotation angles. A similar experiment was made using two different CT volumes of the same patient. With one volume as the pre-operative CT volume, and the other one to generate synthetic CT fluoroscopy images, similar results were obtained.

The second experiment was performed with CT fluoroscopy images from a respiratory motion simulator. As shown in Fig. 7, the target organ had one degree of freedom and was moved by a motor in the cranio-caudal direction. After a pre-operative volumetric scan was obtained, the data was saved in DICOM format with 512 x 512 resolution, 1mm slice thickness and 0.74 mm pixel size. The motor of the simulator was aligned with the CT gantry such that the motion of the phantom was perpendicular to the imaging plane (Fig. 8). Since the organ phantom was rigid, its motion curve was the same as that of the motor. A sequence of CT fluoroscopy images were taken at about 6Hz and saved in the DICOM format. The resolution of the CT fluoroscopy image was 256 x 256, with 10mm slice thickness and 1.48 mm pixel size. A 10mm radius region was selected on the first frame of the CT fluoroscopy image. The motion tracking was initialized. Fig. 9 shows the motion tracking results compared to the known motion curve of the motor at two different motion modes. The major motion in the Z direction (perpendicular to the imaging plane) was very consistent with the motion curve of the motor. The maximum displacement in X and Y directions was under 0.8 mm and treated as noise. The average position error was under 1mm, if the delay in time is ignored. As might be expected, the tracking algorithm tended to have a small position error when the target's motion was slow or close to zero.
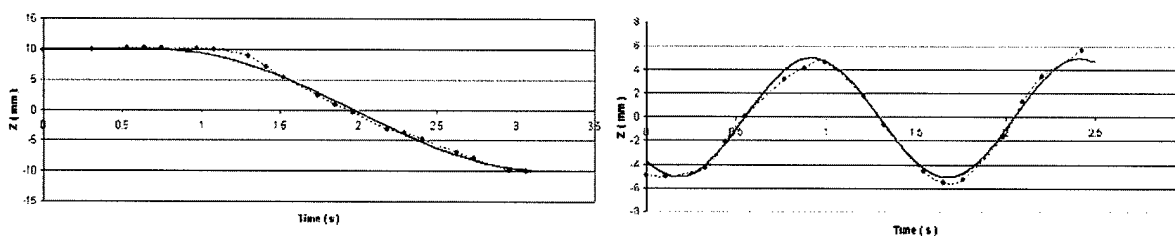

Fig.9 Experimental results of simulator test. The left and right curves show the displacement of the target organ at two different motions. The displacement in Z direction is compared to the ground truth of the motion curve of the phantom.
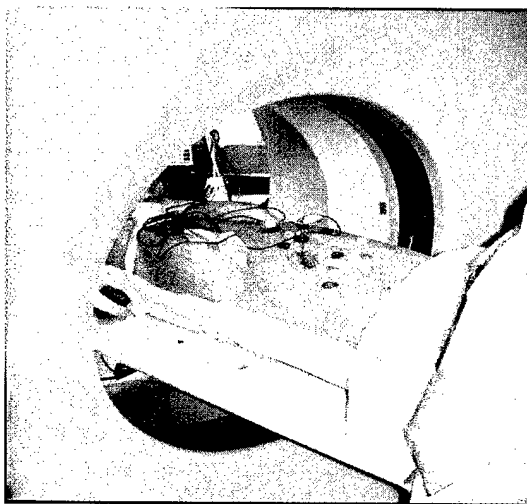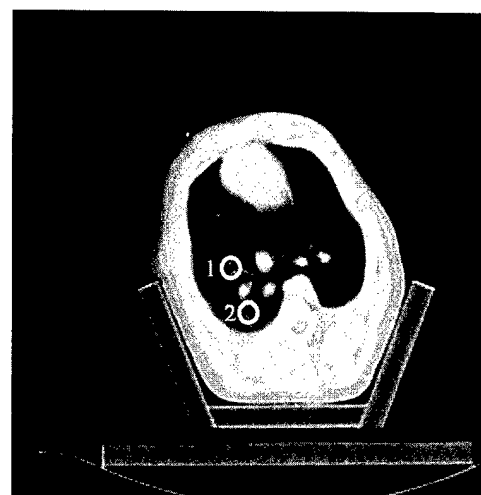
Fig.10 Swine study

Fig.11 CT fluoroscopy image of Swine study

The third experiment was a swine study (Fig. 10). This study was done under an approved animal care protocol. Most of the parameters were the same as the second experiment except that the pixel size was 0.47 mm for the preoperative CT image and 1.48 mm for the CT fluoroscopy image. The respiratory rate was set at 11 cycles per minute using a ventilator. Instead of using the frame grabber, the CT fluoroscopy images were obtained from the DICOM files saved by the CT. Since the CT machine can only save about the last twenty frames of CT fluoroscopy images, only a portion of the respiratory cycle was recorded. Fig. 12 shows the trajectories of two different locations of the CT fluoroscopy image during the respiratory cycle. The curves on the left and right correspond to the regions 1 and 2 in Fig. 11 respectively. While the motion patterns are similar in some respects, there are enough differences to note that different regions in the lung (even regions that are close by) will move with different patterns. With a 2G Hz Pentium 4 CPU, the frequency of the tracking algorithm was between 2Hz and 3Hz. The algorithm worked for most of the lung region. For some regions with little texture, the SSD algorithm failed, most likely because it did not have enough information to uniquely determine the match of the CT fluoroscopy image region in the CT volume.
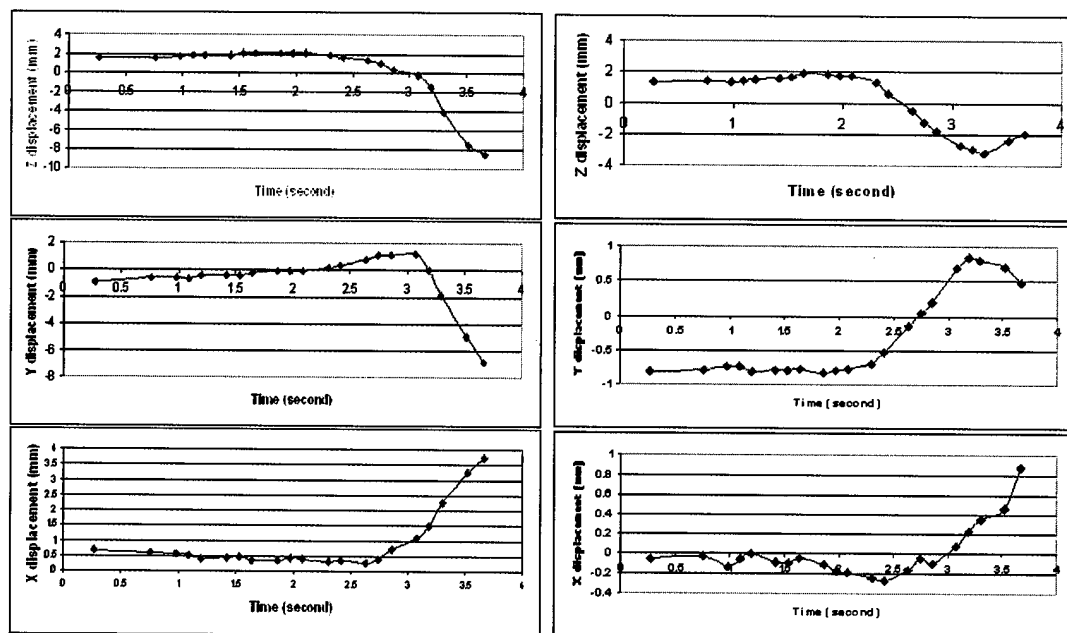

Fig.12 Motion estimation. The pictures on the left / right shows the motion curves of region 1 / 2 in Fig. 11.

4. DISCUSSION

The basic assumption of region-based tracking methods is that the image pixels inside the tracking region undergo a single affine transformation. This assumption is often violated by the lung region. The disadvantage of such an approach is the lack of resolution – a fixed region size means that the approach cannot adapt to the underlying data [13]. One way to improve the algorithm is to use more sophisticated deformable model such as spline deformation rather than the affine transformation. As a result, the analysis region can be bigger, which should also make the algorithm more robust. Another problem that may affect the accuracy is that, instead of tracking the target lesion directly, the algorithm tracks the region inside the CT fluoroscopy imaging plane. If the local rigidity assumption of tracking region and the target lesion is violated, more error will be introduced.

Compared to the conventional motion tracking problem in computer vision, the tracking problem of this paper has the following properties:
(1) since the CT fluoroscopy image region changes over time, the matching template is not fixed, and the efficient tracking algorithm presented in [2] cannot apply;
(2) there is no illumination change in the problem. Instead, the difference between CT images and CT fluoroscopy images needs to be adjusted;
(3) the algorithm does not need to deal with the object occlusion. The lack of texture and large deformation are the major reasons to lose the tracking.

Experimental results showed that the algorithm worked reasonably well in most of the lung area. At some locations where there was not much texture, the algorithm could not track the target. This could be mitigated by selecting a region close to the target lesion that the algorithm is able to track, and use that region to infer the location of the target. In addition, the algorithm can be combined with other methods to increase its robustness. For instance, we can track the motion of the chest wall and try to correlate this motion with the motion of the target lesion. In case the SSD algorithm fails, the motion of the chest wall may be able to be used to estimate the motion of the target lesion.

In order to evaluate the algorithm, it is desirable to use a second tracking method to obtain the ground truth of the target motion. However, this is often impractical. For example, although the magnetic tracker can track the motion of the internal organ, its performance is very poor in a CT scanner. Currently, we are trying to get a 4D CT dataset [14] to evaluate the algorithm.

Our future work will focus on improving the robustness of the algorithm. A post-failure recovery strategy should be established. Chest wall motion tracking and its correspondence to the target lesion will be investigated. Additional animal studies are also planned.

5. CONCLUSION

This paper presented a new algorithm to track the motion of pulmonary lesions using CT fluoroscopy. Initial experimental results showed that the algorithm worked well with a respiratory motion simulator and has reasonable performance in a swine study. Future experiments are planned to incorporate the algorithm with the robotically assisted lung biopsy system.

To the best of the authors' knowledge, there are no other published methods that are non-invasive and can track pulmonary lesions at any location of the lung. The algorithm is automated and can run in nearly real-time. Although the current speed of the algorithm (2-3Hz) is not fast enough to keep up with the CT fluoroscopy update rate (6 Hz), with a faster CPU and the optimization of the algorithm, it is hoped that the algorithm will work in real-time.

ACKNOWLEDGMENT

REFERENCES

1. J. M. Rehg, A.P. Witkin, "Visual tracking with deformation models", Proc. IEEE intl. Conf. On *Robotics and Automation*, vol.1, 844-850, IEEE, Sacramento, CA, USA, 1991.

2. G. Hager and P. Belhumeur, "Efficient Region Tracking With Parametric Models of Geometry and Illumination", *IEEE Trans. on Pattern Analysis and Machine Intelligence*, vol. 20(10): 1205-1039, 1998.

3. J. Shi and C. Tomasi, "Good features to track", IEEE Conf. On *Computer Vision and Pattern Recognition*, 593-600, IEEE, Seattle, WA, USA, 1994.

4. R. Szeliski and J. Coughlan, "Spline-based image registration", *Intl. J. of Computer Vision*, vol. 22, 199-218, 1997.

5. M. Gleicher, "Projective Registration with Difference Decomposition", IEEE Conf. On *Computer Vision and Pattern Recognition*, 331-337, IEEE, San Juan, Puerto Rico, 1997.

6. K. Toyama and G. Hager, "Incremental Focus of Attention for Robust Vision-Based Tracking", *Int. J. Computer Vision*, 35(1), 45-63, 1999

7. B. McCane, B. Galvin, K. Novins, "Algorithmic Fusion for More Robust Feature Tracking", *Intl. J. of Computer Vision*, vol. 49(1), 79-89, 2002.

8. Y. Chen, Y. Lin and S. Y. Kung, "A Feature Tracking Algorithm Using Neighborhood Relaxation With Multi-Candidate Pre-Screening", Proc. of IEEE Int'l Conf. on *Image Processing*, vol. II, 513--516, IEEE, Lausanne, Switzerland ,1996.

9. J. J. More, "The Levenberg-Marquardt Algorithm: Implementation and Theory, in Numerical Analysis", *Lecture Notes in Mathematics*, vol. 630, G. A. Watson, ed., 105-116, Springer-Verlag, Berlin, 1977.

10. J. V. Hajnal, D. L.G. Hill, D. J. Hawkes, *Medical Image Registration*, CRC Press LLC, 2001.

11. S Hu and E. A. Hoffman, "Automatic Lung Segmentation for Accurate Quantitation of Volumetric X-Ray CT Images", *IEEE Trans. Medical Imaging*, vol. 20(6), 2001.

12. M. Kohler, *Using the Kalman Filter to track Human Interactive Motion Modeling and Initialization of the Kalman Filter for Translational Motion*, Technical Report, 1997.

13. S. Krüger, *Motion Analysis and Estimation using Multiresolution Affine Models, Ph.D. thesis*, 1998.

14. D. A. Low, M. Nystrom, E. Kalinin, and P. Parikh, "A method for the reconstruction of four-dimensional synchronized CT scans acquired during free breathing", Medical physics, 30(6), 1254-63, 2003.